Figure 10. Single-molecule imaging of GFP–STAT1.

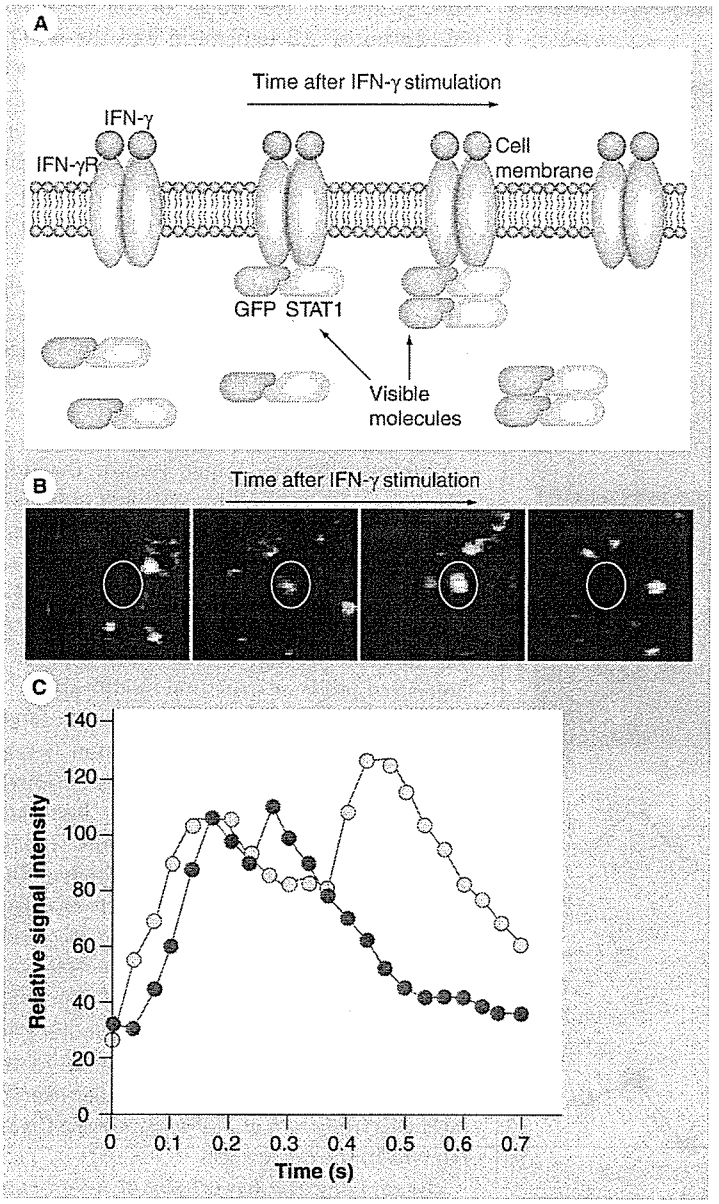

(A) Scheme of GFP–STAT1 behavior. **(B)** A single molecule imaging of GFP–STAT1 in HeLa cells. Fluorescent signal of a single GFP–STAT1 molecule attached to the cell membrane can be observed after IFN-γ stimulation was visualized sequentially. A GFP–STAT1 signal appeared in the time-lapse images (seen in the circles). **(C)** The signal intensity of every GFP–STAT1 molecule in the video images was measured and plotted (n = 2). These curves showed two peaks, indicating that two GFP–STAT1 molecules were bound to the same portion.
GFP: Green fluorescent protein; IFN: Interferon; STAT: Signal transducer and activator of transcription.

Conclusion

Observation is the beginning of science, especially in biology and the life sciences. Modern cell biologists or bioscientists have analyzed molecules and their interplay by using conventional separation methods with a large number of cells. When we do this, what we find is different from what we envisaged, based on previous knowledge.

In nanomedicine, as in nanoregenerative medicine, nanodrug delivery or any other nanotherapy, a clear image of morphological dynamism and its molecular mechanism at the cellular level is very important in order to proceed in new ways. The difference between our usual imaging systems and videovisualization is the clear existence of a time axis and its objectiveness. We usually watch living events for a certain time and can then understand their task-oriented movements and processes over time. Video imaging will also record unexpected findings and recognitions.

In addition, we are in an age when we can analyze molecular species, structures and their quantity by sensitive mass spectrometry from small to large molecular sizes with the aid of conventional bioanalytical methods, such as 2D gel electrophoresis and liquid chromatography [39,40]. Then, for determining a new molecular mechanism, we will combine the knowledge with visualization and molecular analysis. At this stage, single-molecular imaging can be useful and direct for visualizing the molecular functions and the unexpected precise molecular mechanism.

Future perspective

Methodology should be reliable and hopefully simple and easy. Visualizing methods have been, and will continue to be simple, and to be developed rapidly. Rapidly expanding information technologies will also accelerate developments. Therefore, viewpoint-aimed automated visualization methods will also be introduced into life sciences and medicinal research. For example, automated morphological evaluation and diagnosis for many objects will be developed in a visual way because it is simple to explain and also direct.

However, it will take a little more time to make molecular analysis easy and simple. MS is sensitive and useful for quantitative and qualitative analysis of biomolecules; however, at this stage, this method still needs skills, knowledge and further experiences. By establishing a fundamental and simplified base for structure analysis, this method will become much more popular for medical researchers.

The development of combination or simultaneous analysis between visualization and molecular analysis should also be developed soon. We have proposed video-mass-scope and are now

Figure 11. Quinacrine uptake into RBL-2H3 cells.

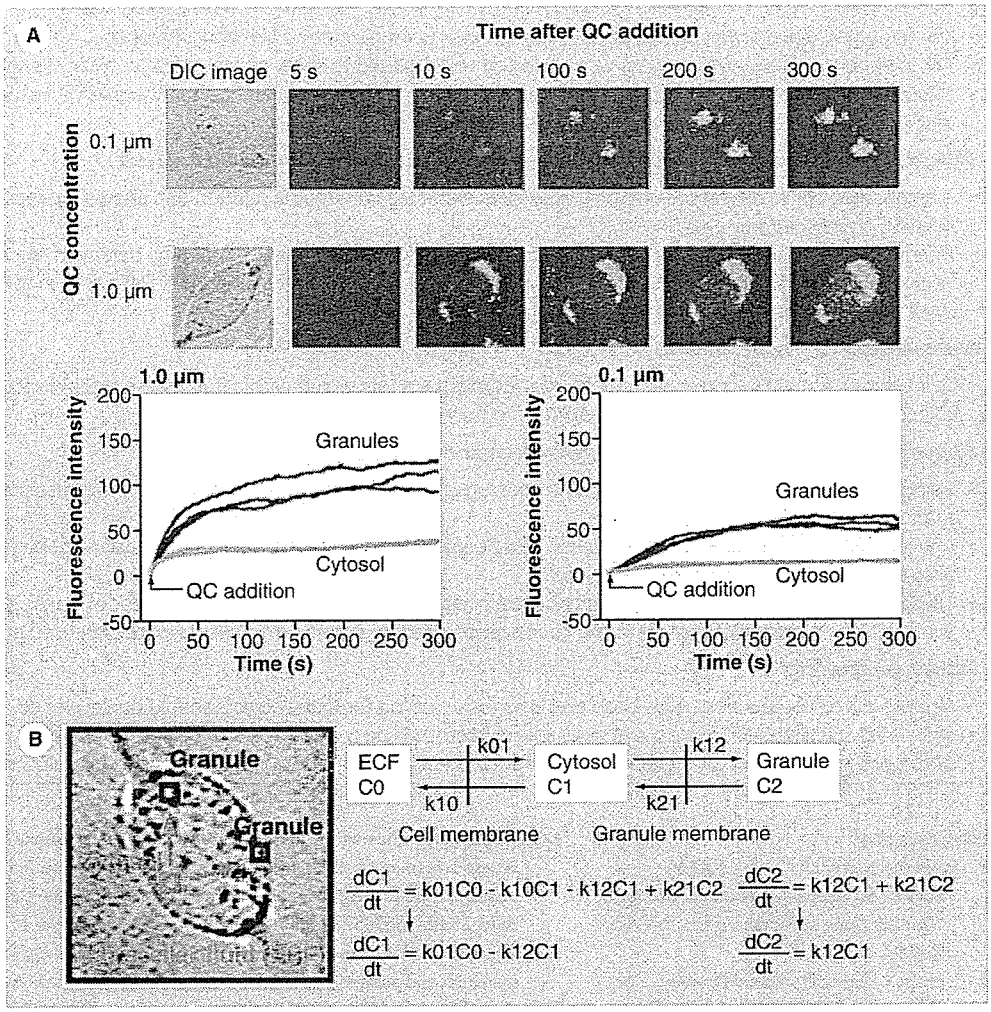

(A) Upper pictures show DIC illumination images of analyzed RBL-2H3 cells before QC addition and time-lapse fluorescent images presented in grayscale after 0.1 µmol/l QC addition. In the lower graphs, fluorescence intensity of selected areas in the cytosol and microgranules (three areas each) after 1 µmol/l QC addition is plotted. The arrows show the time of QC addition. **(B)** Scheme of QC uptake analysis. The areas of fluorescent signal analysis were selected as indicated. QC transport was analyzed using a two-compartmental model. The formula of the model was simplified.
DIC: Differential interference contrast; QC: Quinacrine.

introducing robotics as an interface between video microscope and MS for removing the sample from a cell and following sample pretreatment for mass analysis. In the mass spectroscopic field, 2D mass imaging of sliced samples is now popular [16,24,42–44]. These couple to perhaps make the next step simple and easy in future methodologies. More target-tracing dynamic visualization is also required for nanomedicine. Micro-positron emission tomography and micro-MRI at high spatial resolution are required and should be developed in this field [45,46].

Observation is direct and the results are easy to understand; however, unfortunately we cannot 'watch' molecular structures. Therfore, we require a method of analyzing the molecule and its function. We hope we will soon be in the age when we can proceed to visual nanomedicine.

Acknowledgement

This work was supported partly by Grant-in-Aid for Scientific Research from the Ministry of Education, Science and Culture, Japan, and Grant-in-Aid for Research group (H16-Kodomo-012) from the Ministry of Health, Labor and Welfare of Japan.

Executive summary

Microvisualization of cell dynamism by video microscopes as a morphological approach

- The neutrophil phagocytosis and degranulation process is visualized by a video microscope.
- The eosinophil phagocytosis process was visualized and digitized to show an increased mobility at englobement.
- Degranulation from RBL-2H3 cells was counted from the video image. Numerical data showed that two different signaling mechanisms controlled calcium influx-induced degranulation.

Morphological to molecular analysis: video & mass spectrometry combined analysis

- A single mast cell in the differentiation process was extracted with matrix solution and analyzed directly by mass spectrometry, showing a clear histamine peak.
- Video-mass-scope using a resin-packed elecrospray ionization needle enabled real-time detection of histamine and serotonin release from RBL-2H3 cells together with its morphological changes after stimulation. Different secretion mechanisms between these two molecules were demonstrated.

Nanokinetics for nanomedicine

- Quinacrine transport into the cytosol and microgranules was visualized with a fluorescent video microscope. The kinetics of quinacrine transport could be calculated from the fluorescence intensity.

Single molecular imaging for observing molecular tasks in a cell

- Using single-fiber illumination and a video microscope, movement of cell surface receptors was visualized by labeling an antibody with gold colloids.
- The combination of single-fiber illumination and fluorescent video microscope enabled observation of a YOYO-1-labeled phage DNA molecule showing spring-like behavior.
- Using the same system, a green fluorescent protein-labeled signal transducer and activator of transcription (STAT)1 molecule in a living cell was visualized. Changes in the fluorescence intensity showed that STAT1s were dimerized after stimulation.

Future perspective

- An automated visualization, evaluation and diagnosis method for many objects should be developed.
- A coupled apparatus of imaging and mass spectrometry will be a promising tool for future studies in nanomedicine.
- Micro-positron emission tomography and micro-magnetic resonance imaging at high spatial resolution are needed.

Bibliography

1. Alberts B, Bray D, Lewis J, Raff M, Roberts K, Watson JD: *Molecular Biology Of The Cell.* Garland Publishing Inc., NY, USA (1989).
2. Inoue S, Spring K: *Video Microscopy: The Fundamentals.* Plenum Press, NY, USA (1997).
3. Bowlt C: Measurement of the resolution of the optical microscope. *Phys. Educ.* 18, 178 (1983).
4. Smolyaninov I, Elliott J, Zayats A, Davis C: Far-field optical microscopy with a nanometer-scale resolution based on the in-plane image magnification by surface plasmon polaritons. *Phys. Rev. Lett.* 94, 057401 (2005).
5. Stephens DJ, Allan VJ: Light microscopy techniques for live cell imaging. *Science* 300(5616), 82–86 (2003).
6. Herschman HR: Molecular imaging: looking at problems, seeing solutions. *Science* 302(5645), 605–608 (2003).
7. Suzaki E, Kobayashi H, Kodama Y, Masujima T, Terakawa S: Video-rate dynamics of exocytotic events associated with phagocytosis in neutrophils. *Cell Motil. Cytoskeleton* 38(3), 215–228 (1997).
8. Wardlaw AC, Pillemer L: The properdin system and immunity. V. The bactericidal activity of the properdin system. *J. Exp. Med.* 103(5), 553–575 (1956).
9. Masujima T: Visualized single cell dynamics and analysis of molecular tricks. *Ana. Chim. Acta* 400, 33–43 (1999).
10. Seldin DC, Adelman S, Austen KF *et al.*: Homology of the rat basophilic leukemia cell and the rat mucosal mast cell. *Proc. Natl Acad. Sci. USA* 82(11), 3871–3875 (1985).
11. Ozawa K, Kobayashi H, Kawai E, Suzaki E, Nonomura Y, Masujima T: Quantitative analysis of exocytosis visualized by a video-enhanced light/fluorescence microscope reveals two distinct components of exocytosis in RBL-2H3 cells. *FEBS Lett.* 398(1), 67–73 (1996).
12. Ozawa K, Masujima T, Ikeda K, Kodama Y, Nonomura Y: Different pathways of inhibitory effects of wortmannin on exocytosis are revealed by video-enhanced light microscope. *Biochem. Biophys. Res. Commun.* 222(2), 243–248 (1996).
13. *Methods in Cell Biology (Volume 56). Video Microscopy.* Sluder G, Wolf DE (Ed.). Academic Press, NY, USA (1998).
14. Yamashita M, Fenn JB: Electrospray ion source. Another variation on the free-jet theme. *J. Phys. Chem.* 88, 4451–4459 (1984).
15. Tanaka K, Ido Y, Akita S, Yoshida Y, Yoshida T: Detection of high mass molecules by laser desorption time-of-flight mass spectrometry. *Proc. Second Japan-China Joint Symposium Mass Spectrometry* 185–188 (1987).
16. Reyzer ML, Caprioli RM: MALDI mass spectrometry for direct tissue analysis: a new tool for biomarker discovery. *J. Proteome Res.* 4(4), 1138–1142 (2005).
17. Guerquin-Kern JL, Wu TD, Quintana C, Croisy A: Progress in analytical imaging of the cell by dynamic secondary ion mass spectrometry (SIMS microscopy). *Biochim. Biophys. Acta* 1724(3), 228–238 (2005).
18. Shimizu M, Ojima N, Ohnishi H, Shingaki T, Hirakawa Y, Masujima T: Development of the single-cell MALDI-TOF (matrix-assisted laser desorption/ionization time-of-flight) mass-spectroscopic assay. *Anal. Sci.* 19(1), 49–53 (2003).
19. Shimizu M, Levi-Schaffer F, Ojima N, Shinagaki T, Masujima T: A single-cell matrix-assisted laser desorption/ionization

time-of-flight mass-spectroscopic assay of the cell-maturation process. *Anal. Sci.* 18(1), 107–108 (2002).

20. Colliver TL, Brummel CL, Pacholski ML, Swanek FD, Ewing AG, Winograd N: Atomic and molecular imaging at the single-cell level with TOF-SIMS. *Anal. Chem.* 69(13), 2225–2231 (1997).
21. Li L, Garden RW, Romanova EV, Sweedler JV: *In situ* sequencing of peptides from biological tissues and single cells using MALDI-PSD/CID analysis. *Anal. Chem.* 71(24), 5451–5458 (1999).
22. Li L, Garden RW, Sweedler JV: Single-cell MALDI: a new tool for direct peptide profiling. *Trends Biotechnol.* 18(4), 151–160 (2000).
23. Rubakhin SS, Garden RW, Fuller RR, Sweedler JV: Measuring the peptides in individual organelles with mass spectrometry. *Nat. Biotechnol.* 18(2), 172–175 (2000).
24. Twerenbold D, Caprioli RM, Matter U: Imaging mass spectrometry of a mouse brain. *Macromizer News Ed.* 4, 44–45 (2004).
25. Sirikatitham A, Yamamoto T, Shimizu M, Hasegawa T, Tsuyama N, Masujima T: Resin-packed nanoelectrospray in combination with video-mass-scope for the direct and real-time molecular analysis of mast cells. *Rapid Commun. Mass Spectrom.* (2006) (In Press).
26. Gatlin CL, Kleemann GR, Hays LG, Link AJ, Yates JR III: Protein identification at the low femtomole level from silver-stained gels using a new fritless electrospray interface for liquid chromatography-microspray and nanospray mass spectrometry. *Anal. Biochem.* 263(1), 93–101 (1998).
27. Davis MT, Lee TD: Rapid protein identification using a microscale electrospray LC/MS system on an ion trap mass spectrometer. *J. Am. Soc. Mass Spectrom.* 9(3), 194–201 (1998).
28. Ishihama Y, Rappsilber J, Andersen JS, Mann M: Microcolumns with self-assembled particle frits for proteomics. *J. Chromatogr. A* 979(1–2), 233–239 (2002).
29. Kang D, Nam H, Kim YS, Moon MH: Dual-purpose sample trap for on-line strong cation-exchange chromatography/reversed-phase liquid chromatography/tandem mass spectrometry for shotgun proteomics. Application to the human Jurkat T-cell proteome. *J. Chromatogr. A* 1070(1–2), 193–200 (2005).
30. Dahlin AP, Bergstrom SK, Andren PE, Markides KE, Bergquist J: Poly(dimethylsiloxane)-based microchip for two-dimensional solid-phase extraction-capillary electrophoresis with an integrated electrospray emitter tip. *Anal. Chem.* 77(16), 5356–5363 (2005).
31. Funatsu T, Harada Y, Tokunaga M, Saito K, Yanagida T: Imaging of single fluorescent molecules and individual ATP turnovers by single myosin molecules in aqueous solution. *Nature* 374(6522), 555–559 (1995).
32. Nie S, Zare RN: Optical detection of single molecules. *Annu. Rev. Biophys. Biomol. Struct.* 26, 567–596 (1997).
33. Ishijima A, Kojima H, Funatsu T, Tokunaga M, Tanaka H, Yanagida T: Simultaneous observation of individual ATPase and mechanical events by a single myosin molecule during interaction with actin. *Cell* 92(2), 161–171 (1998).
34. Sase I, Miyata H, Ishiwata S, Kinosita K Jr: Axial rotation of sliding actin filaments revealed by single-fluorophore imaging. *Proc. Natl Acad. Sci. USA* 94(11), 5646–5650 (1997).
35. Tokunaga M, Kitamura K, Saito K, Iwane AH, Yanagida T: Single molecule imaging of fluorophores and enzymatic reactions achieved by objective-type total internal reflection fluorescence microscopy. *Biochem. Biophys. Res. Commun.* 235(1), 47–53 (1997).
36. Suzuto M, Hirakawa Y, Ohnishi H, Tachino S, Eyring EM, Masujima T: Nano-kinetics of probe-particles in solution visualized by a pin-fiber video scope. *Anal. Sci.* 19(1), 43–47 (2003).
37. Hirakawa Y, Hasegawa T, Masujima T, Tokunaga M, Tsuyama N, Kawano M: Single-molecule Imaging of protein in living cells by pin-fiber video-microscopy. *Proc. 13th Int. Symp. Biolumin. Chemilumin.* 215–218 (2004).
38. Tamura A, Ozawa K, Ohya T, Tsuyama N, Eyring EM, Masujima T: Nano-kinetics of drug molecule transport into a single cell. *Nanomedicine* 1(3), 345–350 (2006).
39. Darnell JE Jr, Kerr IM, Stark GR: Jak-STAT pathways and transcriptional activation in response to IFNs and other extracellular signaling proteins. *Science* 264(5164), 1415–1421 (1994).
40. Lee KH: Proteomics: a technology-driven and technology-limited discovery science. *Trends Biotechnol.* 19(6), 217–222 (2001).
41. James P: Of genomes and proteomes. *Biochem. Biophys. Res. Commun.* 231(1), 1–6 (1997).
42. Nygren H, Malmberg P, Kriegeskotte C, Arlinghaus HF: Bioimaging TOF-SIMS: localization of cholesterol in rat kidney sections. *FEBS Lett.* 566(1–3), 291–293 (2004).
43. Sjovall P, Lausmaa J, Nygren H, Carlsson L, Malmberg P: Imaging of membrane lipids in single cells by imprint-imaging time-of-flight secondary ion mass spectrometry. *Anal. Chem.* 75(14), 3429–3434 (2003).
44. Brunelle A, Touboul D, Laprevote O: Biological tissue imaging with time-of-flight secondary ion mass spectrometry and cluster ion sources. *J. Mass Spectrom.* 40(8), 985–999 (2005).
45. Herschman HR: Micro-PET imaging and small animal models of disease. *Curr. Opin. Immunol.* 15(4), 378–384 (2003).
46. Chauvaux B, Dereppe JM, Huis R: Micro-imaging by magnetic resonance on flexible polyurethane foams. *Magn. Reson. Imaging* 14(7–8), 937–939 (1996).

Website

101. NIH image
http://rsb.info.nih.gov/nih-image/

Artificially accumulated ß-catenin inhibits proliferation and induces neurite extension of neuroblastoma cell line NB-1 via up-regulation of trkA

SURASAK SANGKHATHAT[1,3], KEIGO NARA[1], TAKESHI KUSAFUKA[2], AKIHIRO YONEDA[1] and MASAHIRO FUKUZAWA[1]

[1]Department of Pediatric Surgery, Osaka University Graduate School of Medicine, 2-2 Yamadaoka, Suita, Osaka 565-0871; [2]Division of Pediatric Surgery, Department of Surgery, Nihon University School of Medicine, 30-1 Oyaguchikami-machi, Itabashi-ku, Tokyo 173-8610, Japan; [3]Pediatric Surgery Unit, Department of Surgery, Faculty of Medicine, Prince of Songkla University, Hadyai, Songkhla, Thailand

Received May 2, 2006; Accepted July 25, 2006

Abstract. Recent evidence suggests an association between up-regulation of ß-catenin/Wnt signaling pathway and neuronal differentiation of neuroblastoma. We overexpressed ß-catenin into a human neuroblastoma cell line NB-1 and observed its effect on cellular morphology, growth potential and alteration in a known differentiation related gene, trkA. Expression plasmids containing wild-type and mutated forms of ß-catenin gene were transfected into NB-1 cells, using liposome-based transfection method. The mutated forms were a deletion of three nucleotides of codon 45 and a large deletion involving the whole exon 3. In the transient transfection model, cell viability assay demonstrated significant negative effect of mutated ß-catenin transfection, but not wild-type, on the cell proliferation. To investigate impacts of ß-catenin overexpression in detail, a stable transfection model was established. Clones with comparable expression of ß-catenin at the mRNA level were selected. Only the selected clones with mutated form of ß-catenin exhibited neurite extension pattern and stunned cell proliferation, in association with higher accumulation of total cellular ß-catenin protein as evidenced by Western blot and immunocytochemistry. Cell cycle progression demonstrated significantly higher G0-G1 fraction in each stable cell clone with ß-catenin expression plasmid. In addition, retarded G1/S transition was observed exclusively in the cell clones with mutated form. Concomitantly with overexpressed ß-catenin, up-regulations of trkA and Ha-ras were also identified. Our study suggests a potential availability of ß-catenin/Wnt signaling pathway as a target of molecular manipulation for treatment of high-risk neuroblastoma and a potential association between the pathway and the trkA/neurotrophin cascades.

Correspondence to: Professor Takeshi Kusafuka, Division of Pediatric Surgery, Department of Surgery, Nihon University School of Medicine, 30-1 Oyaguchikami-machi, Itabashi-ku, Tokyo 173-8610, Japan
E-mail: kusafuka@med.nihon-u.ac.jp

Key words: neuroblastoma, ß-catenin, tyrosine kinase, neuronal differentiation

Introduction

Neuroblastoma is one of human cancers with high diversity of disease progression which is associated with its heterogeneity in the biology (1). Differentiation of malignant neuroblastic cells can be found varying from poorly differentiated neuroblasts to mature ganglion cells. Moreover, inverse relationship between the aggressiveness of a neuroblastoma and its maturation has been well defined in *in vitro* experiments as well as in clinical series (2,3). Undifferentiated neuroblastoma tends to metastasize and responds poorly to chemotherapeutic agents while tumors containing more mature cells are less aggressive. In addition, some neuroblastomas have a potency to regress spontaneously from an undifferentiated state to a completely benign cellular appearance (4,5). Manipulating the level of differentiation in this kind of malignancy is, therefore, one of the molecular therapeutic strategies. Although various extrinsic factors has been demonstrated to induce neuronal differentiation such as transretinoic acid (*t*RA), lithium, and various growth factors (6-8); intrinsic signaling pathways which govern the differentiation process in a neuroblastoma remains less well elucidated.

Roles of tyrosine kinase signaling in growth and differentiation of neuroblastoma have been considerably explored. In this pathway, nerve growth factor (NGF) receptor, tyrosine kinase-A (trkA), is the main player that binds to NGF to activates downstream transcription of genes related to survival or differentiation (1,9). In addition, up-regulation of trkA was also demonstrated in the model of *t*RA induced neuronal differentiation (10).

Wnt-signaling pathway plays an important role in neuronal development process in vertebrates. In the canonical Wnt/ß-catenin cascade, ß-catenin acts as a central molecule that activates transcription of downstream growth-promoting genes.

Intracellular level of ß-catenin is tightly regulated by its phosphorylation through casein kinase and glycogen synthase kinase-3ß (GSK-3ß) (11). ß-catenin is expressed constitutively in neurons and neuroblastoma (12). Lines of evidence suggested that up-regulation of Wnt-signaling pathway has a potential effect on differentiation status of neuroblasts. In mouse neuroblastoma cells treated by lithium chloride, inhibition of GSK-3ß by the chemical compound leads to an accumulation of ß-catenin and morphological differentiation (7). A recent study demonstrated that ß-catenin plays a role in promoting neuronal differentiation of murine neural stem cells (13). Taken together we hypothesized that it should be possible to induce even human neuroblastoma cells into a differentiation process by manipulating ß-catenin itself. In this study, we transfected expression plasmids containing full-length wild-type and mutated ß-catenin into a neuroblastoma cell line NB-1 and found negative impact of overexpression of ß-catenin on cell progression in transient transfection experiments. In stably transfected cell lines, multidirectional neurite extension, together with significant decrease in cellular proliferation rate and retarded cell-cycle progression were observed. Moreover, alteration in the expression of trkA protein and one of its downstream members, Ha-ras, in association with ß-catenin expression suggested a potential link between Wnt signaling and neurotrophin signaling cascades.

Materials and methods

Plasmid construction. Plasmid pEGFP-C1-BCAT-wt and pEGFP-C1-BCAT-del Exon3 were constructed by cloning cDNA sequence of wild-type ß-catenin and ß-catenin with a large deletion on its exon 3, respectively, into a vector pEGFP-C1 (BD Biosciences Clontech, Palo Alto, CA, USA). The cDNA sequences were derived from digestion of plasmids pUHD10-3-BCAT-wt, and pUHD10-3-BCAT-del Exon3 [kindly provided by Dr Yataka Nagasawa, Biomedical Research Center, Osaka University, Japan (14)] with restriction enzymes *Sac*II and *Bam*HI. Subcloning of the ß-catenin sequences into pEGFP-C1 was done following digestion of the vector with the same enzymes. To construct pEGFP-C1-BCAT-delTCT45, a plasmid with a deletion mutation at codon 45 on exon 3 of ß-catenin sequence, pEGFP-C1-BCAT-wt was used as a template for the mutagenesis experiment, using QuickChange™ site-directed mutagenesis kit (Stratagene, Cedar Creek, TX, USA), following the manufacturer's instructions. Blank vector pEGFP-C1 was employed as a mock control.

Cell culture. Human neuroblastoma cells, NB 1 (Riken Cell Bank, Ibaraki, Japan), were cultured in Dubecco's modified Eagle's medium (DMEM, Nacali Tesque, Kyoto, Japan) supplemented with 10% fetal bovine serum (FBS, Cellect, MP Biomedical, Inc., Eschwege, Germany) and 100 U/ml penicillin, 100 μg/ml streptomycin (Nacali Tesque), in humidified 5% CO_2 at 37°C. The cells were fed every 3 days and subcultured at 80% confluence.

Transient transfection experiments

WST-1 assay of cell viability after transient transfection with ß-catenin plasmid. To study effects of various types of ß-catenin overexpression in NB1 cells, transient transfection experiment was done. Briefly, cells were seeded on a 96-well plate at the density of 10^4 cells/well. Simultaneously with seeding, transfection of each plasmid was done by using TransIT-Neural reagent (Mirus Corp., Madison, WI, USA) at the concentration of 0.15 μg of plasmid/10 μl of transfection reagent/well. Twenty-four hours later, a follow-on transfection was repeated with the same mixture. With this transfection protocol, the efficiency was approximately 30-40% as evaluated by a transfection of blank pEGFP vector (data not shown). To determine cell progression ability in each transfection group, WST-1 viability assay (Nacali Tesque) was performed at day 3, 5 and 7 post-transfection. After 10 μl of WST-1 solution was added to each well, the plate was incubated at 37°C. The absorbency of the treated samples against blank controls was measured with an immunoreader (Immuno Mini NJ-2300, Nippon Inter-Med K.K., Tokyo, Japan) with 414 nm as a detection wavelength and 630 nm as a reference wavelength.

Gene expression assays by real-time reverse transcription-polymerase chain reaction (RT-PCR). Total cellular RNA was prepared by RNAqueous RNA isolation kit (Ambion, Austin, TX, USA), according to the manufacturer's protocol. First-strand cDNA was synthesized from 1 μg of total-RNA using MMLV Reverse Transcriptase (Clontech Laboratories, Palo Alto, CA, USA) and oligo(dT) primers. Twenty-four hours prior to transfection, $5x10^5$ cells of NB-1 were seeded in each well of a 6-well plate. Transfection was performed in the same protocol as for the transient transfection model described above. After 48 h, cells were harvested for RNA extraction and cDNA synthesis. To quantitate the level of mRNA of ß-catenin, real-time RT-PCR was performed on an ABI PRISM 7700 Sequence Detection System together with Sequence Detector V1.7 software (PE Applied Biosystems, Inc., San Jose, CA, USA). Primers and TaqMan probes used in this study were presented previously (15). Human GAPDH was used as an internal control. The mRNA copy numbers of ß-catenin were standardized by the copy number of GAPDH in each sample.

Stable transfection model

Selection of stably transfected cell lines. Cells were seeded at $1.5x10^5$ cells/well in 6-well plate. Each plasmid (3 μg) was incubated with 6 μl of TransIT-Neural reagent in 200 μl of serum-free media for 15 min before adding to each well. Approximately 24 h after the transfection, expression of green fluorescent protein was checked under an ultraviolet microscope and the culture media were then replaced by selection media containing 750 μg/ml of G418 (geneticin, Nacali Tesque). Cells were maintained in the selection media for at least 14 days. The isolated G418 resistant cell clones were then selected and amplified in the media with 500 μg/ml of G418.

To confirm the existence of transfected ß-catenin gene, DNA was extracted from each selected cell clone with High Pure PCR template preparation kit (Roche Inc., Indianapolis, IN, USA), following the supplier's instructions. PCR was performed using the primer set BCAT3/4 (16,17) which were placed on exon 2 and 4, flanking the whole length of exon 3. In a cell colony with extrinsically transfected ß-catenin

sequence, an additional smaller PCR product band of cDNA size (either wild-type or truncated size) appears whereas in a parental cell line and the cell colonies stably transfected with blank GFP vector, PCR gave only a single large band amplified from genomic DNA (data not shown). The smaller band from each sample was cut and the genotype confirmed by direct sequencing. Cell clones with comparable expression level of ß-catenin at the mRNA level as verified by real-time RT-PCR were selected from each group. Selected stable cell clones with empty pEGFP-C1, pEGFP-C1-BCAT-wt, pEGFP-C1-BCAT-delTCT45 and pEGFP-C1-BCAT-del Exon3 were designated as mock, wild-type, del-TCT45 and del-Exon3, respectively.

Immunocytochemistry and cytochemistry. Stably transfected cells in each group were plated on a 4-chamber glass slide (BD Falcon, Becton-Dickinson & Co., San Jose, CA, USA) at the density of 10^5 cells/chamber. Four days after plating, cells were fixed in 4% paraformaldehyde and slides were rinsed in PBS, permeabilized with 1% Triton X-100 for 1 h, then blocked with 10% normal rabbit serum for 30 min before incubation with anti-ß-catenin antibody (0.5 μg/ml; Transduction Laboratories, Lexington, KY, USA) overnight at 4°C. For visualization, FITC-conjugated rabbit anti-mouse immunoglobulins (6 mg/ml; Dako, Glostrup, Denmark) were used as second antibody. To study the change in cell morphology, slides were incubated in PBS containing 0.002% of Phalloidin-Tetramethylrhodamine-B-isothiocyanate (TRTC) (Sigma-Aldrich Corp., St. Louis, MO, USA) in order to stain filamentous actin, followed by 0.02% diamidino-2-phenylindole (Nacali Tesque) for nuclear staining, then washed and mounted with fluorescence mounting medium (DakoCytomation, Tokyo, Japan). Photography was taken with Keyence VB6000 digital photography system (Keyence, Tokyo, Japan) attached to Nikon Eclipse C1000 microscope (Nikon, Tokyo, Japan). Negative control neglected the ß-catenin antibody, but followed the other staining procedures.

Study of ß-catenin protein alteration and simultaneous change of trkA and Ha-ras expression by Western blotting. Total cellular extracts from each stably transfected line were collected using RIPA lysis buffer (Upstate, Lake Placid, NY) supplemented with protease inhibitor cocktails. Insoluble material was removed by centrifugation at 14,000 x g for 10 min, and the supernatant was used for Western blot analysis. Protein concentration was determined with the BCA protein assay set (Pierce, Rockford, IL, USA). Approximately 20 μg of total protein were loaded into each lane on a 10% sodium dodecyl sulfate-polyacrylamide gel electrophoresis and subsequently transferred onto a polyvinyl difluoride membrane. The membrane was incubated with primary antibody for 1 h at room temperature. Primary antibodies used in this study were anti-ß-catenin monoclonal antibody (Transduction Laboratories) at a dilution of 0.5 μg/ml, trkA (H-190) polyclonal antibody (0.2 μg/ml, Santa Cruz Biotechnology, Inc. Santa Cruz, CA, USA), and Ha-ras (C20) polyclonal antibody (0.2 μg/ml, Santa Cruz Biotechnology, Inc.). The membrane was then washed three times and incubated with the horseradish peroxidase conjugated antibody of appropriate species (Dako) for 1 h. After three washes with TBS, the signals were developed using an enhanced chemiluminescence system (ECL plus, Amersham Biosciences, Inc., Piscataway, NJ, USA) and visualized after exposure to Hyperfilm (Amersham Biosciences, Inc.).

Growth study by trypan blue exclusion technique. To study the growth characteristic of each stable cell clone, $5x10^4$ cells from each clone group were plated in triplicate in 1 ml of complete media in 24-well plates. Cells were trypsinized and then counted every 24 h for 10 days using a hemocytometer and trypan blue exclusion technique.

Cell cycle analysis. Each stably transfected NB-1 clone ($3x10^5$ cells/well) was seeded in a 6-well plate. At 24, 48 and 72 h, the cells were washed twice with ice-cold PBS, harvested, fixed with ice-cold PBS in 70% ethanol, and stored at 4°C. For a flow cytometric analysis, the cells were incubated with 0.1 mg/ml RNase-A at 37°C for 30 min, stained with 50 μg/ml propidium iodide for 30 min on ice, and then measured using a FACScan flow cytometer (Becton-Dickinson, Franklin Lakes, NJ, USA) with CellQuest software. Analysis of cell cycle was assisted with FlowJo v.4.4.4 software (Tree Star Inc., Ashland, OR, USA). The experiments were performed three times and the average values are presented.

Apoptosis evaluation. For stable cell clones, apoptosis assay was performed semi-quantitatively by using ApopTag Plus Fluorescein *In Situ* apoptosis detection kit (Serologicals Corp., Norcross, GA, USA), according to the manufacturer's protocol which is based on TUNEL principle. Briefly, cells were seeded in equal amount in four-chamber glass slides. After 3 days, slides were fixed with paraformaldehyde and subsequently reacted with dioxygenin-labeled terminal deoxynucleotidyl transferase, followed by fluorescein conjugated anti-dioxygenin antibody binding. Positive cells harboring apoptotic bodies were counted under a fluorescence microscope.

Evaluation of reversibility of ß-catenin effect on proliferation by ß-catenin siRNA transfection. Del-TCT45 cells were plated at the density of 10^4 cells/well in a 96-well plate. ß-catenin siRNA oligonucleotides (SMARTpool, Dharmacon, Lafayatte, CO, USA) were transfected using HiPerFect transfection reagent (Qiagen, Inc., Valencia, CA, USA) at the final concentration of 100 nM of siRNA in serum-free DMEM. Details regarding sequences of siRNA can be found in our previous report (15). Sham transfection using HiPerFect alone and transfection of negative control siRNA (B-Bridge International, Inc., Sunnyvale, CA, USA), which has no significant homology to any known sequences in human genome, were also performed. On the third day of treatment, comparative cell progression was evaluated by WST-1 viability assay.

To evaluate knock-down efficiency at the mRNA level, $5x10^5$ cells were seeded on each well of a 6-well plate. siRNA treatment including controls was applied in the same protocol as above. Cells were harvested at 48 h after the treatment for RNA extraction and real-time RT-PCR.

Data analysis and statistics. Unless stated otherwise, all experiments were performed in triplicate under similar

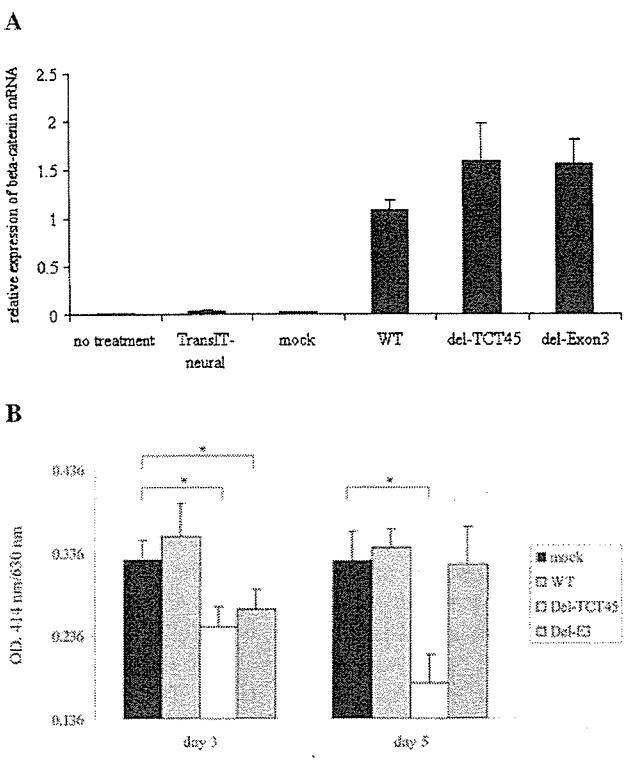

Figure 1. (A), Results of real-time RT-PCR demonstrating mRNA expression of ß-catenin relative to GADPH in NB-1 cells increased in comparable levels in all three groups transfected with ß-catenin expression plasmid. (B), WST-1 assay demonstrated significant lower amount of viable cells in those groups transfected with point-mutated and large truncated ß-catenin (del-TCT45 and del-Exon3 plasmids) (*p-value <0.01).

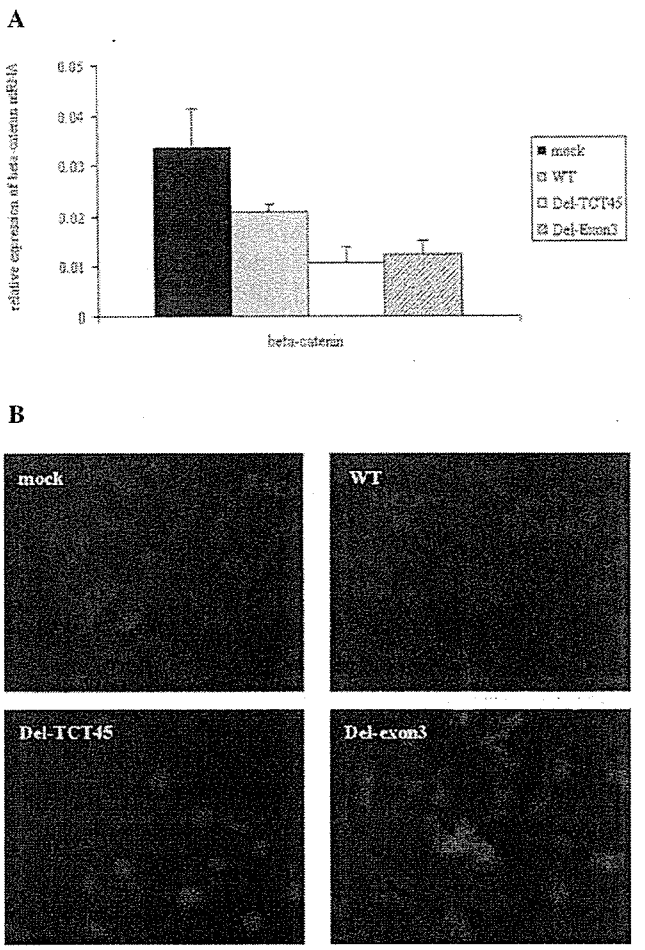

Figure 2. (A), Average relative expression of stable clones in each transfection group which showed slightly lower mean expression level in cell groups that were transfected with del-TCT45 and del-Exon3 plasmids. (B), Conversely, ß-catenin immunoreactivity in the del-TCT45 and the del-Exon3 was paradoxically more intense than the mock and the wildtype groups. Note that the localization of ß-catenin in mock control was mostly membrane localization whereas in the del-TCT45 and the del-Exon3, accumulation appeared at the cytoplasm and the cell nucleus.

conditions. Data are presented as means together with standard deviation for each parameter. The statistical analysis was performed by the unpaired Student's t-test, and statistical significance was considered when the p-value was <0.05 or 0.01, as appropriate.

Results

Overexpression of ß-catenin suppressed proliferation of NB-1 cells. After transfection, mRNA expression of ß-catenin in NB-1 cells increased in comparable levels in all three groups transfected with ß-catenin expression plasmid (Fig. 1A). Synchronous with this overexpression, WST-1 assay demonstrated significant lower amount of viable cells in those groups transfected with point-mutated and large truncated ß-catenin (del-TCT45 and del-Exon3) (Fig. 1B). It was noted that the group transfected with point-mutated plasmid exhibited stronger and longer growth inhibition effect than the plasmid with whole exon truncation.

Accumulation of ß-catenin protein in stable clones with mutated ß-catenin plasmid. In the stable transfection model, cell clones with comparable expression of ß-catenin were selected from each group. Real-time RT-PCR revealed slightly lower mean expression level of ß-catenin in cell groups that were transfected with del-TCT45 and del-Exon3 plasmids (Fig. 2A). Western blot study showed higher amount of ß-catenin protein in the del-TCT45 and del-Exon3 clones (Fig. 3), which was consistent with immunocytochemistry results that demon-strated more intense immunoreactivity in those cell clones (Fig. 2B).

Growth retardation in NB-1 cells harboring artificial ß-catenin expression was associated with an inhibition at G1/S phase transition. The growth study confirmed growth retardation in clones harboring mutated catenin (Fig. 6). At 48-h of seeding, the flow cytometry revealed a higher average G0-G1 phase fraction in all three clones transfected with ß-catenin expression plasmid (Fig. 4A). In addition, a significant retardation of G1/S transition was observed in the two groups harboring mutated forms of ß-catenin (Fig. 4B).

Multidirectional neurite extension in ß-catenin transfected NB-1. Multidirectional neurite extension of NB-1 was observed in 2 groups of cell clone transfected with mutated ß-catenin (del-TCT45 and del-Exon3) (Fig. 5). The same pattern of

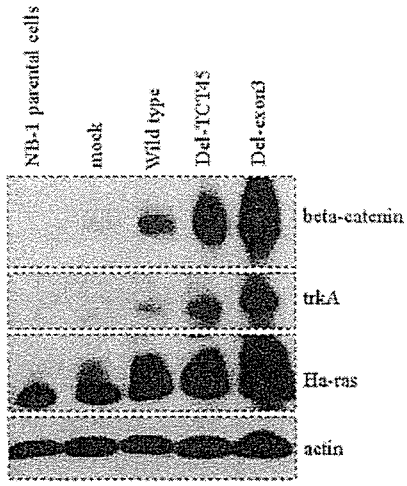

Figure 3. Western blot showed increased ß-catenin protein in two groups of stable clone transfected with mutated ß-catenin plasmid. Concomitantly with overexpression of ß-catenin protein, increased expressions of trkA and Ha-ras were identified.

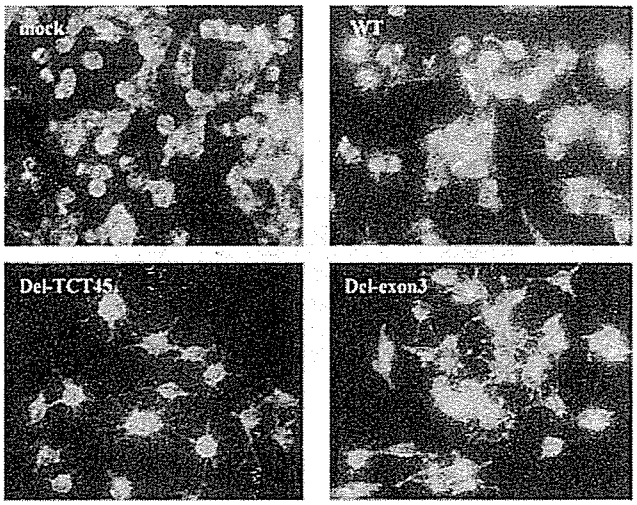

Figure 5. Phalloidin-TRTC staining of NB-1 exhibited multidirectional neurite extension of NB-1 was observed in two groups of cell clone transfected with mutated ß-catenin (lower panel). The same pattern of morphologic change was found in stable clones transfected with wild-type ß-catenin plasmid, but to a lesser extent.

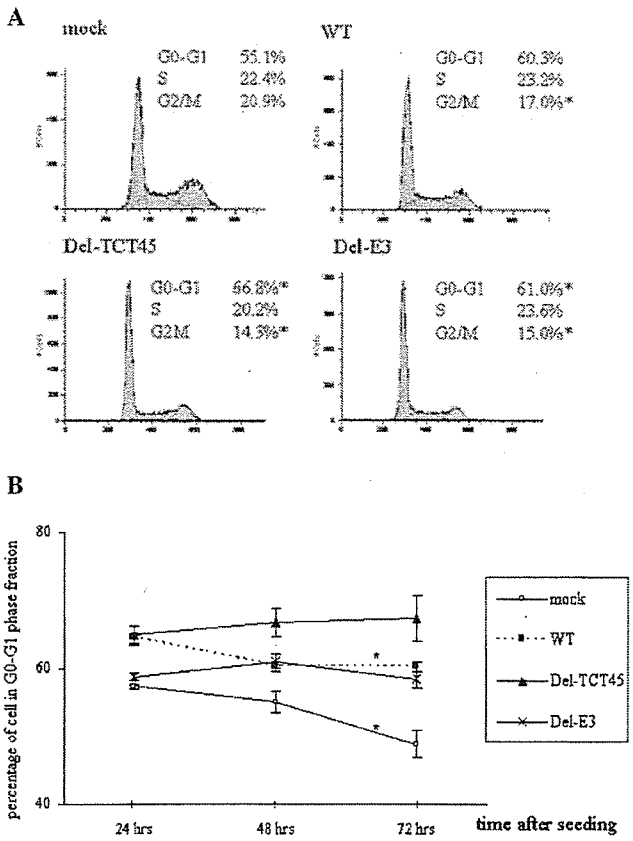

Figure 4. (A), Cell-cycle study by propidium iodide staining revealed significantly higher average G0-G1 phase fraction in all groups with ß-catenin plasmid (*P-value <0.05 when compared to mock). (B), Time-course study showed retardation of G0-G1 decline in the del-TCT45 and the del-Exon3 groups. Average percentage of G0-G1 fraction at 72 h in mock and wild-type groups reduced significantly when compared with 24-h (*p-value <0.05), however, there was no significant change of the values in the del-TCT45 and the del-Exon3 groups.

morphologic change could be found in stable clones transfected with wild-type ß-catenin plasmid, but to a lesser extent.

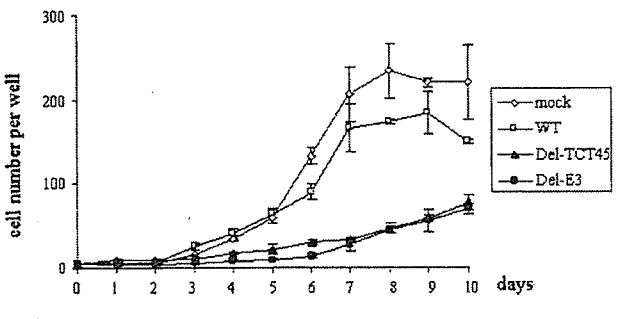

Figure 6. Time-course curve of growth comparison of stably transfected clones, using direct counting trypan blue exclusion. The study demonstrated significantly slower proliferation rate in the two groups with mutated ß-catenin.

Up-regulation of trkA and Ha-ras in cell clones with ß-catenin accumulation. Western blot revealed increased expression of trkA and Ha-ras in all groups transfected with ß-catenin expression plasmid (Fig. 3). The alteration of trkA was more obvious in clone groups transfected with mutated forms. Expression of Ha-ras was most intense in the clone transfected with large deletion form of ß-catenin.

Apoptosis was not increased in cell clones with ß-catenin accumulation. The study found lower than three apoptotic bodies per high power field in each group of NB-1 cell clones and there was no difference among the groups.

Growth suppression in the del-TCT45 cell clone could be reversed by ß-catenin siRNA. Real-time RT-PCR confirmed the efficiency of siRNA in post-transcriptional knock-down of ß-catenin expression to 16% of the control level (Fig. 7A). This reduction resulted in significantly higher cell viability in the treatment group (Fig. 7B).

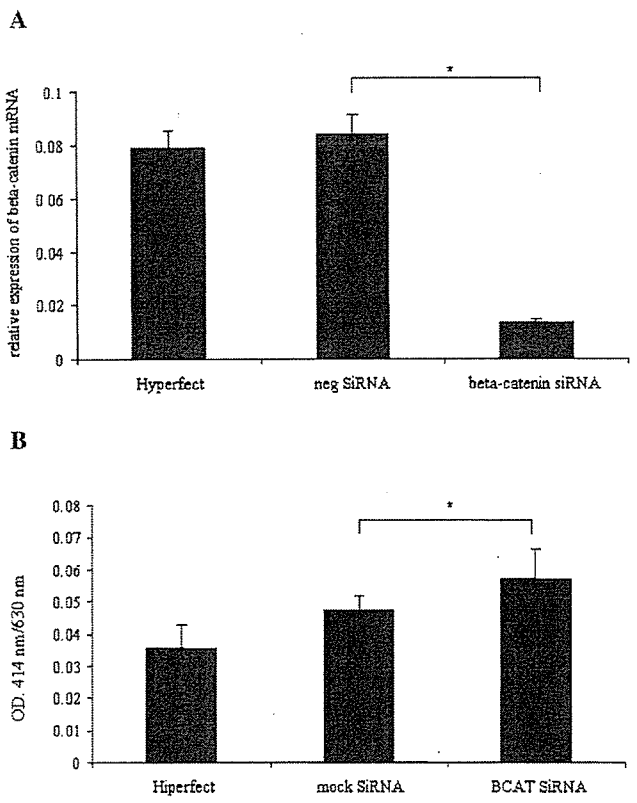

Figure 7. (A), A set of real-time RT-PCR results demonstrating reduction of ß-catenin expression at the mRNA level when a clone of Del-TCT45 was transfected with ß-catenin siRNA. (B), Significantly positive change was seen in the treatment group as investigated by WST-1 (*p-value <0.05).

Discussion

Although neuroblastoma cells harbor uncontrolled proliferation and aggressive characteristic of malignancy, the behavior of developing neuron are retained in many aspects. Neuronal differentiation is one of the characteristics found to be varying from an individual tumor to another (3,5). Correlation between level of differentiation and disease prognosis has been well addressed in clinical studies (2,3).

Molecular mechanism regulating changes in cell morphology and growth in differentiation of neuroblastoma has not been thoroughly clarified, however, it is generally accepted that differentiation occur accompanied with an arrest of proliferation or escape from cell cycle (18). Certain extrinsic factors induce differentiation of neuroblastoma cells and one of the prototypes is *t*RA, the mechanism of which is partly associated with increased expression of membranous receptor trkA. A previous study demonstrated that treatment with lithium chloride induced morphological differentiation of mouse neuroblastoma Neuro 2A cells (7). The study also found that neurite extension in lithium-treated cells was preceded by an accumulation of ß-catenin via an inhibition of GSK-3ß and subsequent accumulation of ß-catenin. In our study, a model of ß-catenin accumulation was directly created in a human neuroblastoma cell line, NB-1, by forced expression of degradation-resistant forms of ß-catenin.

We employed NB-1 in our model as this cell line is derived from human neuroblastoma with MYCN amplification and homozygous deletion of chromosome 1p (19), hence it represents tumors of poor prognosis. Moreover, this cell line is one of a few neuroblastoma cell lines that can be successfully transfected with liposome-based transfection reagent. In comparison with electroporation, less cytotoxicity caused by chemical transfection and considerable transfection efficiency makes the cell line more suitable for a direct study of the impact of extrinsic oligonucleotide induction. With normal culture conditions, the cells appeared as round to polygonal-shaped in monolayer. Neurite outgrowth is not usually found in early days after a subculture. However, we observed that a pattern of the outgrowth in nearly confluent condition was mostly bipolar extension of tough processes, which obviously differed from the multidirectional outgrowth of thin processes as found in our NB-1 lines transfected with ß-catenin. To alleviate the factor of transfection efficiency, we studied alterations in morphology and cell kinetics using a stable transfection model. Western blot study found higher amount of ß-catenin protein accumulation in the groups of cell clone transfected with mutated ß-catenin, which was consistent with the immunostaining results. The phenomenon was concordant with the expectation that mutation involving the phosphorylation sites inhibits the degradation cascade and leads to stabilization and accumulation of ß-catenin protein.

On transient transfection, although the transfection efficiency was limited, it was demonstrated that proliferation of tumor cells was significantly inhibited in the group overexpressed with mutated ß-catenin. Moreover, this inhibition was reversible when ß-catenin was knocked-down in stably overexpressed clones. Taken together with the observation that cells in those groups harboring ß-catenin accumulation exhibited neurite extension, we postulate that ß-catenin accumulation may provide certain effects on neuronal differentiation. The hypothesis was supported by a recent study which demonstrated a role of ß-catenin/Wnt signaling pathway in differentiation of neural stem cells (13).

Our growth study in stable transfected clones demonstrated obviously slower proliferation rate in cell clones with mutated ß-catenin. This result differed from that of transient transfection model, in which growth suppression effect of del-E3 plasmid appeared milder than del-TCT45. The disparity was possibly the result of a minute difference in transfection efficiency or inequality in cellular reaction to each plasmid. The cell cycle study suggested that the growth retardation was a result of G1/S transition defect which could be shown in groups of cell clone transfected with mutated form of ß-catenin. Based on cytometric evidence alone, although we cannot explain the negative growth effect of neuroblastoma cells by the cell-cycle exit and acquisition to the differentiation process, the pattern of cell-kinetics alteration was similar to that reported in trkA overexpressed cells in the presence of NGF (20). Taken together with our evidence of increased trkA expression in ß-catenin overexpressed groups, it could be postulated that ß-catenin indirectly enhanced differentiation in the NB-1 neuroblastoma cells, through an activation of NGF/trkA pathway.

Role of tyrosine kinase-A (trkA) in promoting morphologic differentiation and growth inhibition in neuroblastoma cell lines has been well defined (21). To promote neuronal

differentiation, trkA functions in concert with its ligand NGF through autophosphorylation and downstream activation of several downstream genes including ras and mitogen-activated protein kinase 1. Increased expression of Ha-ras detected in our study confirmed the up-regulation of the signaling pathway and suggested a possible association between Wnt/ß-catenin and NGF/trkA cascades.

A previous study reported no significant effect of direct ß-catenin overexpression in a neuroblastoma cell line N2A cell, in terms of morphological differentiation (22), for which the authors explained that the experiments were performed in serum-free condition. The findings support our postulation that ß-catenin induced morphological differentiation through an increased expression of trkA, which functions in the presence of its ligand NGF. Further study in more detail is necessary to verify this potential connection.

In summary, our study demonstrated that accumulation of ß-catenin in a neuroblastoma cells led to growth inhibition and neurite extension which was related to up-regulation of trkA. The data suggest a possible availability of ß-catenin as a molecular target for manipulation in the management of neuroblastoma.

Acknowledgements

This study was partially supported by a Grant-in-Aid from the Ministry of Education, Sciences, Sports and Culture of Japan (Grant no. 6591785). S.S. is supported by the Royal Thai Government via the Faculty of Medicine, Prince of Songkla University, Thailand.

References

1. Brodeur GM: Neuroblastoma: biological insights into a clinical enigma (Review). Nat Rev Cancer 3: 203-216, 2003.
2. Shimada H, Umehara S, Monobe Y, Hachitanda Y, Nakagawa A, Goto S, Gerbing RB, Stram DO, Lukens JN and Matthay KK: International neuroblastoma pathology classification for prognostic evaluation of patients with peripheral neuroblastic tumors: a report from the Children's Cancer Group. Cancer 92: 2451-2461, 2001.
3. Chatten J, Shimada H, Sather HN, Wong KY, Siegel SE and Hammond GD: Prognostic value of histopathology in advanced neuroblastoma: a report from the Childrens Cancer Study Group. Hum Pathol 19: 1187-1198, 1988.
4. Haas D, Ablin AR, Miller C, Zoger S and Matthay KK: Complete pathologic maturation and regression of stage IVS neuroblastoma without treatment. Cancer 62: 818-825, 1988.
5. Ambros PF, Ambros IM, Strehl S, Bauer S, Luegmayr A, Kovar H, Ladenstein R, Fink FM, Horcher E, Printz G, Mutz I, Schilling F, Urban C and Gadner H: Regression and progression in neuroblastoma. Does genetics predict tumour behaviour? Eur J Cancer 31A: 510-515, 1995.
6. Sidell N, Altman A, Haussler MR and Seeger RC: Effects of retinoic acid (RA) on the growth and phenotypic expression of several human neuroblastoma cell lines. Exp Cell Res 148: 21-30, 1983.
7. Garcia-Perez J, Avila J and Diaz-Nido J: Lithium induces morphological differentiation of mouse neuroblastoma cells. J Neurosci Res 57: 261-270, 1999.
8. Edsjo A, Nilsson H, Vandesompele J, Karlsson J, Pattyn F, Culp LA, Speleman F and Pahlman S: Neuroblastoma cells with overexpressed MYCN retain their capacity to undergo neuronal differentiation. Lab Invest 84: 406-417, 2004.
9. Maris JM and Mattthay KK: Molecular biology of neuroblastoma. J Clin Oncol 17: 2264-2279, 1999.
10. Bogenmann E, Peterson S, Maekawa K and Matsushima H: Regulation of NGF responsiveness in human neuroblastoma. Oncogene 17: 2367-2376, 1998.
11. Polakis P: Wnt signaling and cancer. Genes Dev 14: 1837-1851, 2000.
12. Satoh J and Kuroda Y: ß-catenin expression in human neural cell lines following exposure to cytokines and growth factors. Neuropathology 20: 113-123, 2000.
13. Israsena N, Hu M, Fu W, Kan L and Kessler JA: The presence of FGF2 signaling determines whether ß-catenin exerts effects on proliferation or neuronal differentiation of neural stem cells. Dev Biol 268: 220-231, 2004.
14. Nagasawa Y, Miyoshi Y, Iwao K, Shinomura Y, Matsuzawa Y and Nakamura Y: Transformation and morphological changes of murine L cells by transfection with a mutated form of beta-catenin. Cancer Res 59: 3539-3542, 1999.
15. Sangkhathat S, Kusafuka T, Miao J, Yoneda A, Nara K, Yamamoto S, Kaneda Y and Fukuzawa M: *In vitro* RNA interference against beta-catenin inhibits the proliferation of pediatric hepatic tumors. Int J Oncol 28: 715-722, 2006.
16. Koch A, Denkhaus D, Albrecht S, Leuschner I, von Schweinitz D and Pietsch T: Childhood hepatoblastomas frequently carry a mutated degradation targeting box of the beta-catenin gene. Cancer Res 59: 269-273, 1999.
17. Udatsu Y, Kusafuka T, Kuroda S, Miao J and Okada A: High frequency of beta-catenin mutations in hepatoblastoma. Pediatr Surg Int 17: 508-512, 2001.
18. Galderisi U, Jori FP and Giordano A: Cell cycle regulation and neuronal differentiation. Oncogene 22: 5298-5219, 2003.
19. Ohira M, Kageyama H, Mihara M, Furuta S, Machida T, Shishikura T, Takayasu H, Islam A, Nakamura Y, Takahashi M, Tomioka N, Sakiyama S, Kaneko Y, Toyoda A, Hattori M, Sakaki Y, Ohki M, Horii A, Soeda E, Inazawa J, Seki N, Kuma H, Nozawa I and Nakagawara A: Identification and characterization of a 500-kb homozygously deleted region at 1p36.2-p36.3 in a neuroblastoma cell line. Oncogene 19: 4302-4307, 2000.
20. Kokunai T, Iguchi H and Tamaki N: Differentiation and growth inhibition of glioma cells induced by transfer of trkA proto-oncogene. J Neurooncol 42: 23-34, 1999.
21. Schramm A, Schulte JH, Astrahantseff K, Apostolov O, Limpt V, Sieverts H, Kuhfittig-Kulle S, Pfeiffer P, Versteeg R and Eggert A: Biological effects of TrkA and TrkB receptor signaling in neuroblastoma. Cancer Lett 228: 143-153, 2005.
22. Fan S, Ramirez SH, Garcia TM and Dewhurst S: Dishevelled promotes neurite outgrowth in neuronal differentiating neuroblastoma 2A cells, via a DIX-domain-dependent pathway. Brain Res Mol Brain Res 132: 38-50, 2004.

Oncogene (2006) 25, 5046–5055

www.nature.com/onc

ORIGINAL ARTICLE

Bcl-2 is a key regulator for the retinoic acid-induced apoptotic cell death in neuroblastoma

H Niizuma[1,2], Y Nakamura[1], T Ozaki[1], H Nakanishi[1], M Ohira[1], E Isogai[1], H Kageyama[1], M Imaizumi[3] and A Nakagawara[1]

[1]Division of Biochemistry, Chiba Cancer Center Research Institute, Chuoh-ku, Chiba, Japan; [2]Department of Pediatrics, Tohoku University School of Medicine, Aoba-ku, Sendai, Japan and [3]Department of Hematology and Oncology, Miyagi Children's Hospital, Aoba-ku, Sendai, Japan

Retinoic acid (RA) has been shown to induce neuronal differentiation and/or apoptosis, and is widely used as a chemotherapeutic agent for treating the patients with neuroblastoma. However, the therapeutic effect of RA is still limited. To unveil the molecular mechanism(s) inducing differentiation and apoptosis in neuroblastoma cells, we compared CHP134 and NB-39-nu cell lines, in which all-*trans*-RA (ATRA) induces apoptosis, with LA-N-5 and RTBM1 cell lines, in which it induces neuronal differentiation. Here, we found that Bcl-2 was strongly downregulated in CHP134 and NB-39-nu cells, whereas it was abundantly expressed in LA-N-5 and RTBM1 cells. ATRA-mediated apoptosis in CHP134 and NB-39-nu cells was associated with a significant activation of caspase-9 and caspase-3 as well as cytoplasmic release of cytochrome *c* from mitochondria in a p53-independent manner. Enforced expression of Bcl-2 significantly inhibited ATRA-mediated apoptosis in CHP134 cells. In addition, treatment of RTBM1 cells with a Bcl-2 inhibitor, HA14-1, enhanced apoptotic response induced by ATRA. Of note, two out of 10 sporadic neuroblastomas expressed *bcl-2* at undetectable levels and underwent cell death in response to ATRA in primary cultures. Thus, our present results suggest that overexpression of Bcl-2 is one of the key mechanisms to give neuroblastoma cells the resistance against ATRA-mediated apoptosis. This may provide a new therapeutic strategy against the ATRA-resistant and aggressive neuroblastomas by combining treatment with ATRA and a Bcl-2 inhibitor.
Oncogene (2006) **25,** 5046–5055. doi:10.1038/sj.onc.1209515; published online 27 March 2006

Keywords: apoptosis; Bcl-2; neuroblastoma; retinoic acid

Correspondence: Dr A Nakagawara, Division of Biochemistry, Chiba Cancer Center Research Institute, 666-2 Nitona, Chuoh-ku, Chiba 260-8717, Japan.
E-mail: akiranak@chiba-cc.jp
Received 8 November 2005; revised 6 February 2006; accepted 15 February 2006; published online 27 March 2006

Introduction

Neuroblastoma, which originates from the sympathoadrenal lineage of the neural crest, is one of the most common solid tumors in childhood and has distinct biological properties in different prognostic subsets (Schor, 1999). For example, tumors in patients less than 1 year of age often regress spontaneously and have a favorable prognosis. In contrast, tumors that occur over 1 year of age display an extensive and metastatic disease at diagnosis, and are often aggressive with an unfavorable prognosis despite an intensive therapy (Brodeur and Nakagawara, 1992). Each of those subsets shows various distinct genetic features including the ploidy status, *MYCN* amplification, allelic loss of the distal part of chromosome 1p and the gain of chromosome 17q (Brodeur, 2003). Additionally, high expression levels of neurotrophin receptors TrkA and TrkB are favorable and unfavorable prognostic indicators of neuroblastomas, respectively (Nakagawara *et al.*, 1993, 1994). Several lines of evidence suggest that the spontaneous regression of the favorable neuroblastomas is attributed at least in part to the developmentally programmed neuronal cell death and/or neuronal differentiation (Nakagawara, 1998). Indeed, the deprivation of nerve growth factor led to the massive cell death through apoptosis of neuroblastoma cells expressing TrkA (Nakagawara *et al.*, 1993).

Retinoic acids (RAs), which appear to be involved in vertebrate morphogenesis, are natural and synthetic derivatives of vitamin A (Maden, 2001; McCaffery *et al.*, 2003), and exert their biological functions through nuclear receptors including RA receptors (RARs) and retinoid X receptors (RXRs) (Lippman and Lotan, 2000). In response to RA binding, RAR/RXR heterodimers regulate the transcription of a number of target genes by binding to the specific DNA response elements (Balmer and Blomhoff, 2002). Retinoic acids have antitumor effects on neuroblastoma-derived cell lines accompanied by a marked decrease in the expression levels of *MYCN* (Thiele *et al.*, 1985). Studies utilizing cell lines also have revealed that neuroblastoma cell lines exposed to all-*trans*-RA (ATRA) undergo neuronal differentiation, cell cycle arrest and/or apoptosis (Melino *et al.*, 1997; van Noesel and Versteeg, 2004). Recent

works offer insights into the molecular mechanisms by which ATRA exerts its biological effects on neuroblastomas. All-*trans*-retinoic acid activates phosphatidylinositol 3′-kinase-Akt pathway that plays an important role in neuronal differentiation (Encinas *et al.*, 1999; Lopez-Carballo *et al.*, 2002), and it reduces the expression levels of MYCN (Thiele *et al.*, 1985) and upregulates the cyclin-dependent kinase (CDK) inhibitor $p27^{KIP1}$ in association with the ATRA-induced cell cycle arrest in neuroblastoma cells (Lee *et al.*, 1996; Nakamura *et al.*, 2003). In addition, certain neuroblastoma cells underwent apoptosis in response to ATRA (Piacentini *et al.*, 1992; Takada *et al.*, 2001; Nagai *et al.*, 2004). Consistent with these observations, 13-*cis*-RA treatment after intensive chemotherapy improved an event-free survival rate of the patients with aggressive neuroblastomas with 17% increase (Villablanca *et al.*, 1995; Matthay *et al.*, 1999). Although the antitumor effects of RA alone on aggressive neuroblastoma are limited, RA treatment has an advantage that it carries no severe side effects. Thus, it is important to enhance the antitumor effects of RA on neuroblastoma cells, and thereby inducing apoptosis.

In the present study, we have found that the ATRA treatment induces neuronal differentiation in neuroblastoma-derived LA-N-5 and RTBM1 cells, whereas CHP134 and NB-39-nu cells undergo p53-independent apoptotic cell death in response to ATRA. Extensive expression studies revealed that the antiapoptotic Bcl-2 was constitutively expressed at high levels in LA-N-5 and RTBM1 cells, whereas CHP134 and NB-39-nu cells expressed Bcl-2 at extremely low levels. Enforced expression of Bcl-2 in CHP134 cells led to a significant inhibition of the ATRA-mediated apoptosis. In accordance with these results, the treatment with Bcl-2 inhibitor in RTBM1 cells resulted in an increased sensitivity to ATRA. Moreover, two out of 10 sporadic neuroblastomas in primary cultures with undetectable *bcl-2* underwent cell death in response to ATRA, whereas seven tumors out of the remaining eight cases expressed high levels of *bcl-2*. These results suggest that Bcl-2 might be a key regulator for the ATRA-mediated apoptotic cell death in neuroblastomas.

Results

ATRA-induced growth inhibition, differentiation and cell death in human neuroblastoma cell lines

To examine the possible effects of ATRA on growth and viability of neuroblastoma cells, human neuroblastoma-derived LA-N-5, RTBM1, CHP134 and NB-39-nu cells were cultured with or without 5 μM of ATRA, and the numbers of viable cells were counted at the indicated time points after the exposure to ATRA. As shown in Figure 1a, ATRA effectively inhibited proliferation of these neuroblastoma cells. Among them, the growth of CHP134 and NB-39-nu cells was much more suppressed in the presence of ATRA. To monitor morphological changes induced by ATRA, ATRA-treated cells were checked by phase-contrast microscopy. As shown in Figure 1b, a neurite outgrowth was evident in ATRA-treated LA-N-5, RTBM1 and CHP134 cells, whereas it was marginal in NB-39-nu cells. Of note, ATRA-induced cell death was detectable in CHP134 and NB-39-nu cells, but not in LA-N-5 and RTBM1 cells. To confirm whether ATRA could induce the apoptotic cell death in CHP134 and NB-39-nu cells, we examined the changes in the number of cells with sub-G1 DNA content in response to ATRA. As shown in Figure 1c and d, the flow cytometric analysis revealed that the number of CHP134 cells with sub-G1 DNA content was significantly increased in response to ATRA. Similarly, ATRA promoted the apoptotic cell death in NB-39-nu cells, albeit to a lesser degree than CHP134 cells. Under our experimental conditions, ATRA failed to induce the apoptotic cell death in LA-N-5 and RTBM1 cells (data not shown).

ATRA-induced apoptotic cell death in neuroblastoma cells

To elucidate the molecular mechanism(s) underlying the ATRA-mediated apoptotic cell death in neuroblastoma cells, we examined whether the procaspases could be proteolytically cleaved to be activated in response to ATRA. To this end, whole-cell lysates prepared from the indicated neuroblastoma cells exposed to 5 μM of ATRA for 0, 2, 4 and 6 days were subjected to immunoblotting with the indicated antibodies. As shown in Figure 2a, the time-dependent proteolytic cleavage of caspase-9 and caspase-3 was observed in CHP134 and NB-39-nu cells, but not in LA-N-5 and RTBM1 cells. Consistent with these results, one of the physiological substrates of the activated caspase-3, poly-ADP-ribose polymerase (PARP), was cleaved in ATRA-treated CHP134 and NB-39-nu cells. In a good agreement with the previous observations showing that caspase-8 is epigenetically silenced in a high percentage of neuroblastoma cells (Teitz *et al.*, 2000; van Noesel *et al.*, 2003), caspase-8 was undetectable in LA-N-5, RTBM1 and CHP134 cells. In contrast, NB-39-nu cells expressed a large amount of procaspase-8. Procaspase-12, which is involved in the endoplasmic reticulum-stress-induced apoptosis (Nakagawa *et al.*, 2000; Morishima *et al.*, 2002), was readily detectable in all of the neuroblastoma cell lines that we examined, and did not respond to ATRA. Under our experimental conditions, ATRA had negligible effects on proteolytic cleavage of caspase-8 and caspase-12 (data not shown).

As caspase-9 is activated in response to the cytoplasmic release of cytochrome *c* from mitochondria, leading to the activation of caspase-3 (Degterev *et al.*, 2003), we sought to examine whether cytochrome *c* could be released in response to ATRA. To this end, CHP134 cells were treated with 5 μM of ATRA or left untreated, and cells were incubated with the antibody against cytochrome *c* or with the control immunoglobulin (Ig)G. Cell nuclei were stained with 4,6-diamidino-2-phenylindole (DAPI). Microscopic images demonstrated that cytochrome *c* staining displays a punctuate

cytoplasmic pattern in the absence of ATRA (Figure 2b, left). This staining pattern was almost identical to the MitoTracker staining (data not shown). ATRA treatment for 4 days induced redistribution of cytochrome *c* to a diffused cytoplasmic pattern in cells with apoptotic nuclei (Figure 2b, middle), suggesting

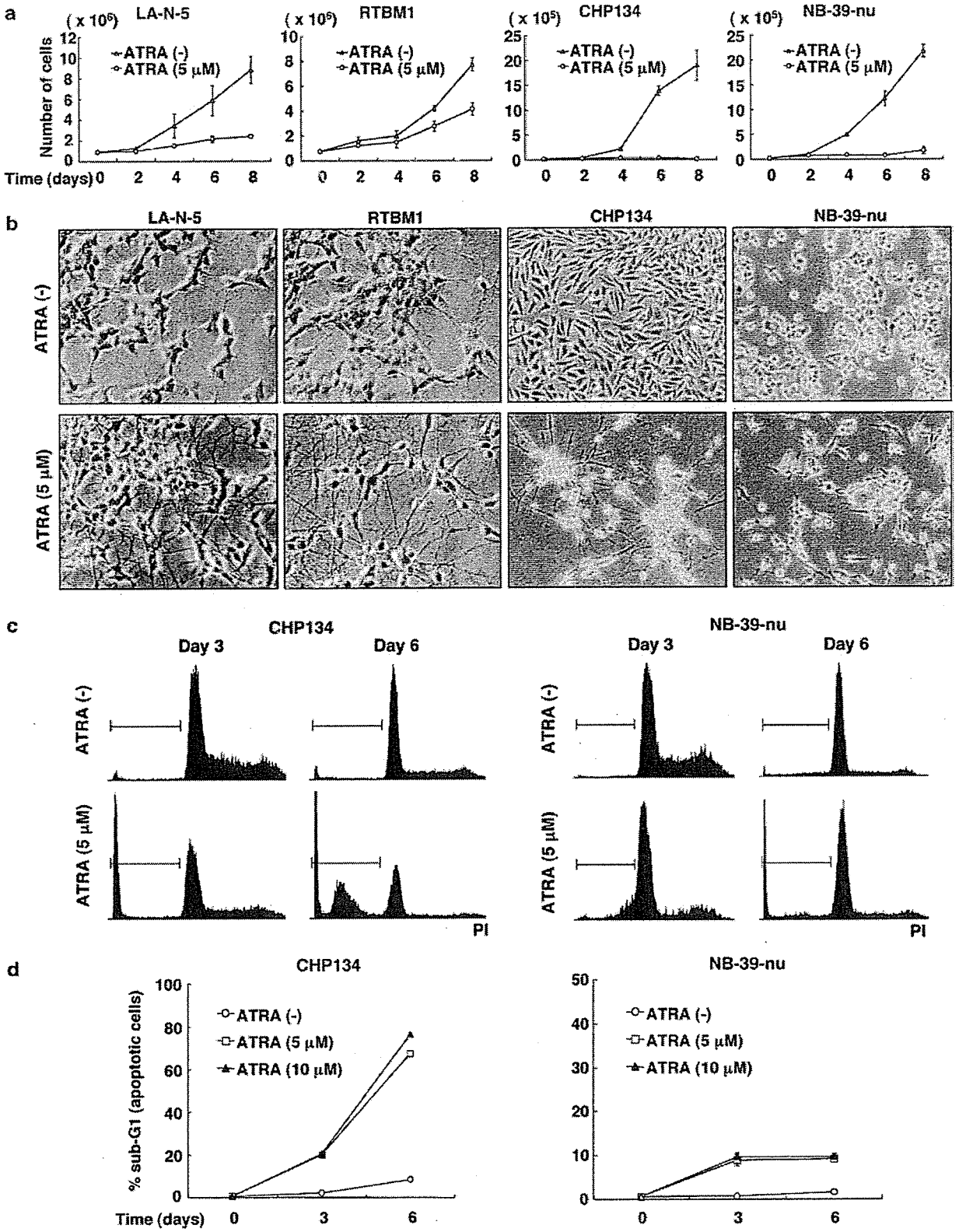

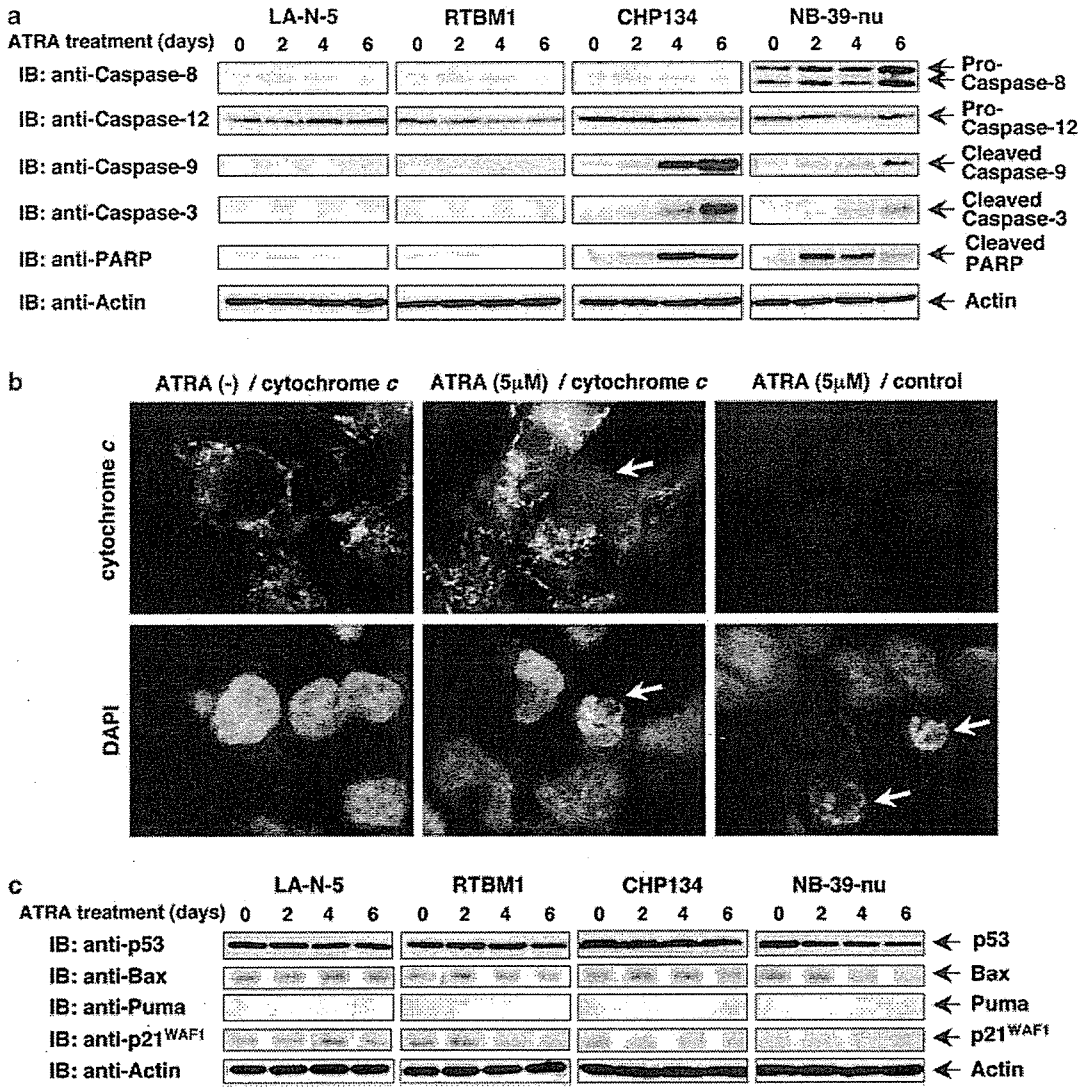

Figure 2 Caspase-9 and caspase-3 are cleaved during the all-*trans* retinoic acid (ATRA)-mediated apoptosis in CHP134 and NB-39-nu cells. (**a**) Immunoblot analysis for various caspases and poly-ADP-ribose polymerase (PARP) in response to ATRA. The indicated neuroblastoma cell lines were treated with 5 μM of ATRA or left untreated. At the indicated time points after the treatment with ATRA, whole-cell lysates were prepared, and analysed by immunoblotting with indicated antibodies. Actin expression was used as a loading control (bottom). (**b**) ATRA-induced cytoplasmic release of cytochrome *c* in CHP134 cells. CHP134 cells were seeded onto coverslips, and cultured in the presence or absence of 5 μM of ATRA. Four days after the treatment with ATRA, cells were fixed and stained with a monoclonal antibody against cytochrome *c* (top, left and middle) or with a normal mouse IgG (top, right). The cell nuclei were stained with 4,6-diamidino-2-phenylindole (DAPI) (bottom). The arrows indicate apoptotic cells with condensed and fragmented nuclei. (**c**) Expression levels of p53 and its direct target gene products in response to ATRA. At the indicated time periods after the treatment with ATRA, whole-cell lysates were prepared, and subjected to immunoblotting with antibodies against p53, Bax, Puma, $p21^{WAF1}$ and actin. Immunoblotting for actin is shown as a control for protein loading (bottom).

Figure 1 Effects of all-*trans* retinoic acid (ATRA) on cell proliferation of LA-N-5, RTBM1, CHP134 and NB-39-nu neuroblastoma-derived cell lines. (**a**) Growth curves of the indicated neuroblastoma cell lines in the presence or absence of ATRA. Cells were grown in the standard culture medium, and treated with 5 μM of ATRA. At the indicated time points after the treatment with ATRA, cells were trypsinized, harvested and number of viable cells was counted in triplicate. (**b**) ATRA-induced morphological changes of neuroblastoma cell lines. Cells were exposed to ATRA at a final concentration of 5 μM or left untreated. Six days after the treatment with ATRA, cells were examined by phase-contrast microscopy. (**c** and **d**) ATRA-induced cell death through apoptosis in CHP134 and NB-39-nu cells. Cells were treated with the indicated concentrations of ATRA or left untreated, and incubated for up to 6 days. At the indicated time points after the treatment with ATRA, cells were collected, fixed and stained with propidium iodide (PI). The DNA content of the cells was then examined by flow cytometry (**c**). The number of cells with sub-G1 DNA content was counted in triplicate (**d**).

that cytochrome *c* release from mitochondria might play an important role in ATRA-induced apoptotic cell death in neuroblastoma cells.

As the neuroblastoma cell lines that we examined carry wild-type p53 (data not shown), we investigated whether p53 could contribute to the ATRA-mediated apoptotic cell death. For this purpose, whole-cell lysates prepared from the indicated neuroblastoma cells exposed to 5 μM of ATRA for 0, 2, 4 and 6 days were processed for immunoblotting with the indicated antibodies. As shown in Figure 2c, the amounts of p53 remained unchanged or slightly decreased after ATRA treatment. In accordance with these results, ATRA had undetectable effects on the expression levels of p53-responsible Bax, Puma and $p21^{WAF1}$, which are implicated in the p53-dependent apoptosis and/or cell cycle arrest (Culmsee and Mattson, 2005). In addition, ATRA failed to induce the phosphorylation of p53 at Ser-15 (data not shown). Thus, it is likely that ATRA-mediated apoptotic cell death in neuroblastoma cells may be regulated in a p53-independent manner.

Differential expression of antiapoptotic Bcl-2 in neuroblastoma cells

To investigate the regulatory mechanisms of apoptotic response to ATRA in neuroblastoma cells, we examined the expression levels of Bcl-2 family proteins, which directly control the mitochondrial pathway of apoptosis. It is worth noting that antiapoptotic Bcl-2 was constitutively expressed at high levels in LA-N-5 as well as RTBM1 cells, whereas CHP134 and NB-39-nu cells expressed Bcl-2 at extremely low levels (Figure 3a). Antiapoptotic Bcl-x_L was expressed at low levels in all cell lines examined. In accordance with the previous observations showing that proapoptotic Bim and Bmf are highly expressed in neuronal cells (Puthalakath *et al*., 2001; Okuno *et al*., 2004; Shi *et al*., 2004), Bim and Bmf were expressed at high levels in all of the cell lines that we examined, but their expression levels remained unchanged in the presence of ATRA.

To determine whether Bcl-2 could contribute to the acquisition of the ATRA-resistant phenotype of neuroblastoma cells, CHP134 cells were transfected with the expression plasmid for Bcl-2 or with the empty plasmid, and their sensitivity to ATRA was examined by flow cytometry. As shown in Figure 3b, Bcl-2 was successfully overexpressed in CHP134 cells as examined by immunoblotting. Interestingly, enforced expression of Bcl-2 inhibited the ATRA-mediated proteolytic cleavage of caspase-3. Consistent with these results, flow cytometric analysis demonstrated that ectopic expression of Bcl-2 significantly reduced the number of cells with sub-G1 DNA content induced by ATRA treatment (Figure 3c and d), suggesting that Bcl-2 might play a critical role in the regulation of apoptotic cell death in neuroblastoma cells.

To further confirm this possibility, we examined the effects of the Bcl-2 inhibitor HA14-1 (Wang *et al*., 2000) on the ATRA-mediated apoptotic response of neuroblastoma cells. RTBM1 cells were treated with 5 μM of ATRA or left untreated for 6 days, and then incubated in the presence or absence of HA14-1 (15, 30 or 50 μM) for 3 h. Phase-contrast microscopic analysis showed that the incubation with ATRA followed by HA14-1 treatment significantly enhanced the apoptotic response of RTBM1 cells, whereas HA14-1 treatment alone increased the number of apoptotic cells to a lesser degree (Figure 4a). Similar results were also obtained by flow cytometric analysis (Figure 4b and c). To examine whether the ATRA-mediated apoptosis in RTBM1 cells induced by HA14-1 treatment could be associated with the activation of the mitochondria-dependent apoptotic pathway, we performed immunoblot analysis. As shown in Figure 4d, HA14-1 treatment at 30 μM or less did not promote the activation of caspase-9 and caspase-3, whereas a small amount of the cleaved caspase-9 and caspase-3 were detectable in RTBM1 cells exposed to 50 μM of HA14-1 alone. Intriguingly, pre-treatment of RTBM1 cells with ATRA enhanced the proteolytic cleavage of caspase-9 and caspase-3 induced by HA14-1 at a final concentration of 50 μM.

To ask whether Bcl-2 could play an important role in ATRA-mediated apoptotic response in primary neuroblastomas, 10 sporadically found neuroblastomas were subjected to both primary culture and reverse transcriptase–polymerase chain reaction (RT-PCR) analysis for *bcl-2*. In five cases, ATRA treatment induced strong outgrowth of neurites as compared with control culture (Figure 5a, left). In the other three cases, ATRA had undetectable effects (data not shown). It is worth noting that many cells underwent cell death after ATRA treatment in the remaining two cases (Figure 5a, right). We also examined the expression levels of *bcl-2* of these 10 primary neuroblastoma samples and four neuroblastoma-derived cell lines by RT–PCR. LA-N-5 and RTBM1 cells abundantly expressed *bcl-2*, whereas CHP134 and NB-39-nu did not (Figure 5b), which was consistent with immunoblotting as shown in Figure 3a. Of particular interest, RT–PCR analysis revealed that two primary cases that underwent cell death in response to ATRA (N-9 and N-10) expressed *bcl-2* at undetectable levels (Figure 5c). In a sharp contrast, the expression of *bcl-2* was detected in the remaining cases, except N-3. Taken together, our present results strongly suggest that Bcl-2 is a key regulator for ATRA-mediated apoptotic cell death in neuroblastoma cells.

Discussion

Retinoic acid is one of the potent antitumor agents that has been used successfully to treat certain human tumors including neuroblastomas (Freemantle *et al*., 2003). Indeed, neuroblastoma patients treated with RA have increased survival rate without severe side effects (Villablanca *et al*., 1995; Matthay *et al*., 1999). Accumulating evidences suggest that RA plays an important role in the regulation of neuroblastoma apoptosis as well as differentiation (Melino *et al*.,

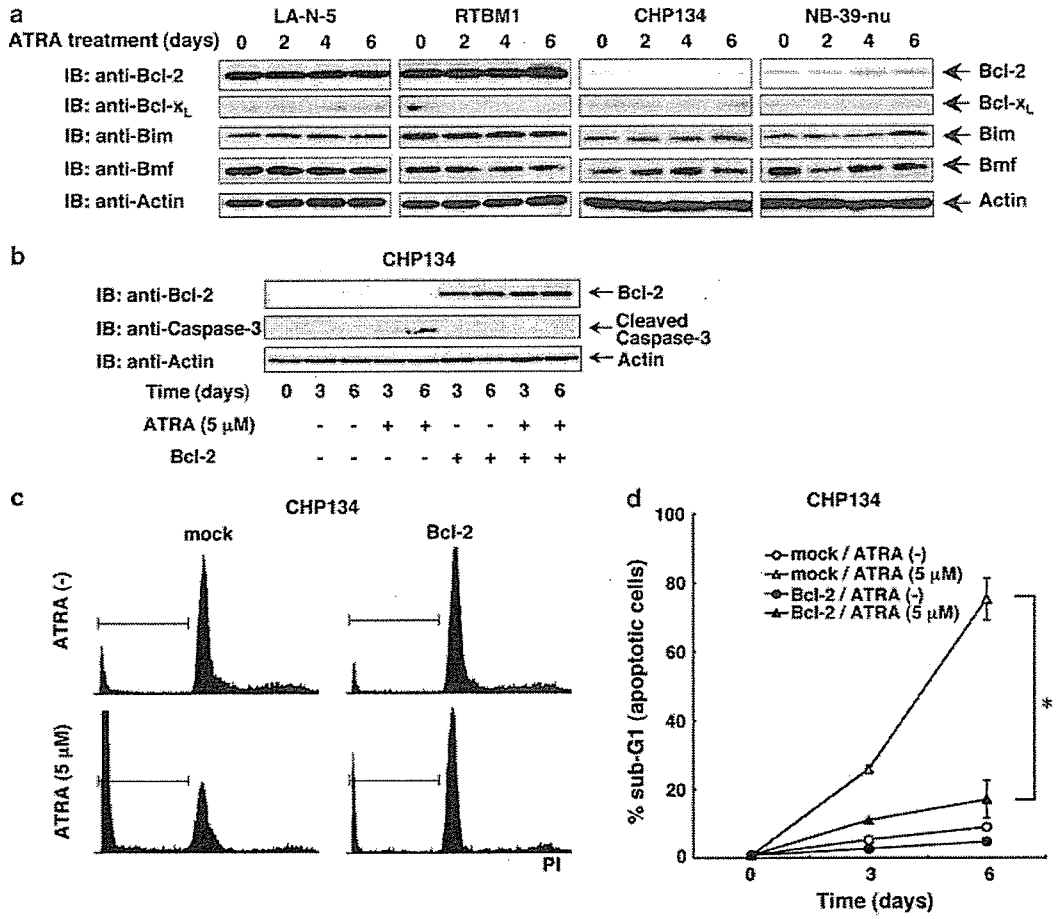

Figure 3 Differential expression of antiapoptotic Bcl-2 protein. (**a**) The indicated neuroblastoma cell lines were cultured in standard culture medium containing all-*trans* retinoic acid (ATRA) at a final concentration of 5 μM. At the indicated time points after the treatment with ATRA, whole-cell lysates were prepared, and analysed by immunoblotting with the antibodies against the indicated Bcl-2 family proteins. Actin expression was examined as a loading control (bottom). (**b**) Overexpression of Bcl-2. CHP134 cells were transiently transfected with the expression plasmid for Bcl-2 or with the empty plasmid. Twelve hours after the transfection, cells were treated with or without 5 μM ATRA, and incubated for additional 3 or 6 days. Whole-cell lysates were prepared, and the expression levels of Bcl-2 (top) and the amounts of the cleaved caspase-3 (middle) were examined by immunoblotting. Actin is shown as a control for protein loading (bottom). (**c** and **d**) Flow cytometry. CHP134 cells were transiently transfected as described in (**b**). At the indicated time periods after the treatment with ATRA, cells were collected, fixed and stained with PI. The DNA content of the cells was examined by flow cytometry. Representative results on day 6 are shown in (**c**). The number of cells with sub-G1 DNA content was counted in triplicate (**d**). *$P<0.01$.

1997; van Noesel and Versteeg, 2004). However, certain neuroblastomas display an RA-resistant phenotype (Reynolds and Lemons, 2001). To further improve the therapeutic effects of RA on neuroblastomas, it is necessary to clarify the detailed molecular mechanisms underlying the RA-mediated neuroblastoma differentiation and/or apoptosis. In the present study, we have found that ATRA causes growth suppression and subsequent neuronal differentiation in human neuroblastoma-derived LA-N-5, RTBM1, CHP134 and NB-39-nu cells to various degrees. Among them, CHP134 and NB-39-nu cells, which express antiapoptotic Bcl-2 at extremely low levels, underwent p53-independent apoptotic cell death in response to ATRA. In contrast, LA-N-5 and RTBM1 cells abundantly expressed Bcl-2, and we did not detect apoptotic cell death upon ATRA treatment. Enforced expression of Bcl-2 in CHP134 cells inhibited the ATRA-mediated apoptosis, and HA14-1-mediated inhibition of the endogenous Bcl-2 in RTBM1 cells enhanced the ATRA-dependent apoptotic cell death. Moreover, studies using primary neuroblastoma tissues showed that ATRA had toxic effect on two out of 10 primary cultures, and these ATRA-sensitive tumors did not express *bcl-2*. Thus, it is likely that antiapoptotic Bcl-2 plays a crucial role in the regulation of the ATRA-mediated apoptotic response in neuroblastomas.

Our present study revealed that neuroblastoma cells can be divided into two groups with respect to the ATRA-induced apoptotic response. CHP134 and NB-39-nu cells underwent apoptotic cell death in response to ATRA, whereas LA-N-5 and RTBM1 cells did not. Consistent with the mitochondria-dependent intrinsic apoptotic pathway of caspase activation (Degterev

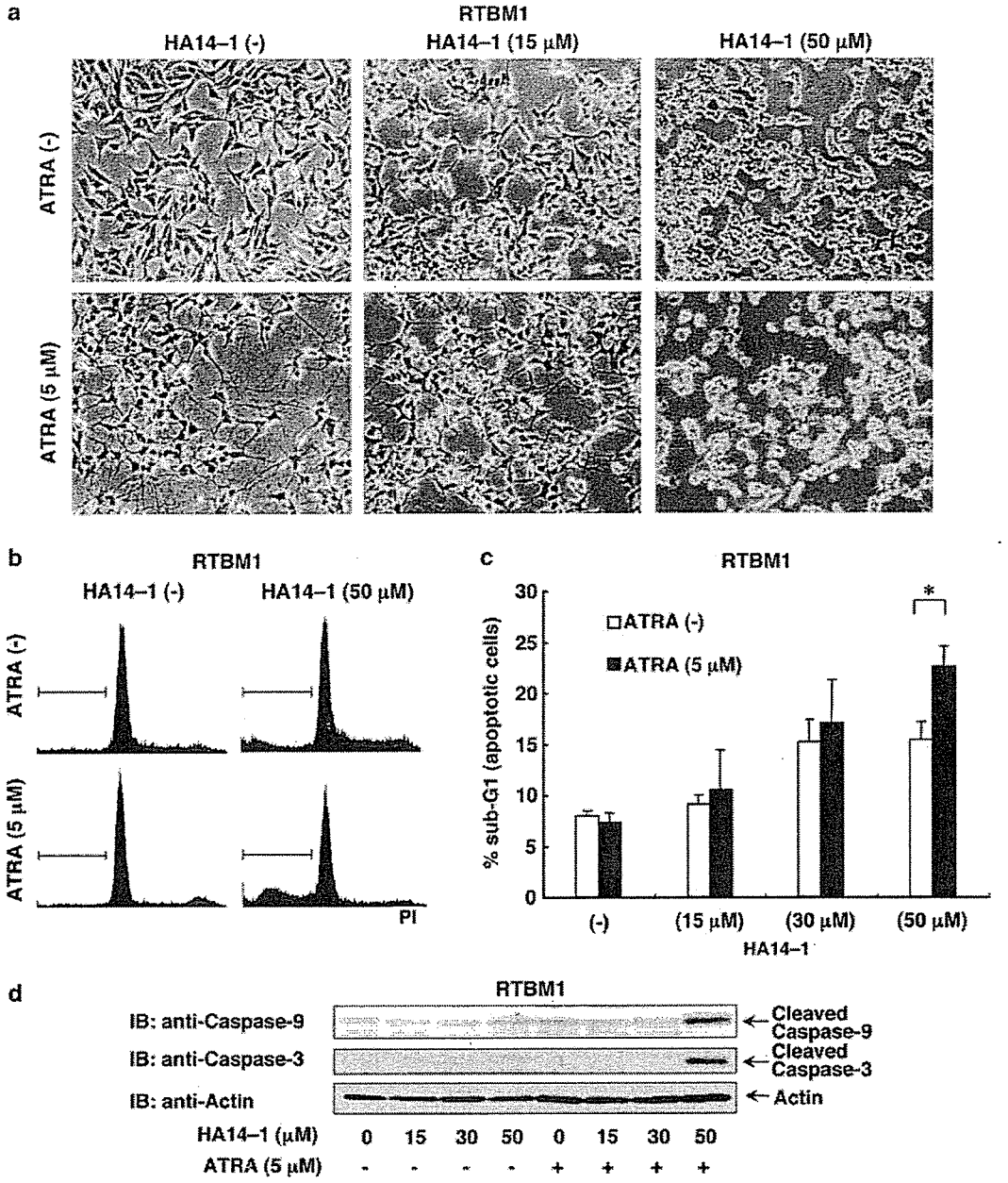

Figure 4 Bcl-2 inhibitor HA14-1 induces apoptosis of all-*trans* retinoic acid (ATRA)-treated RTBM1 cells. (**a**) Morphological changes after HA14-1 treatment of RTBM1 cells. RTBM1 cells were cultured with or without 5 μM ATRA for 6 days in advance, and then treated with HA14-1, a specific inhibitor of Bcl-2, at the indicated concentrations in standard medium for 3 h. Cells were examined by phase-contrast microscopy and photographed after the treatment. (**b** and **c**) FACS analysis. RTBM1 cells were treated with ATRA and HA14-1 as described in (**a**). Cells were collected, fixed and stained with PI. The DNA content of the cells was examined by flow cytometry and representative results are shown in (**b**). The number of cells with sub-G1 DNA content was counted in triplicate (**c**). *$P<0.05$. (**d**) Immunoblotting. Whole-cell lysates of RTBM1 treated with ATRA and HA14-1 were prepared to examine the amounts of cleaved caspase-9 and caspase-3. Actin is shown as a loading control.

et al., 2003), ATRA treatment in CHP134 cells caused a cytoplasmic release of the mitochondrial inter-membrane protein cytochrome *c*, and a sequential proteolytic cleavage of caspase-9, caspase-3 and its physiological substrate PARP. Similar results were obtained in NB-39-nu cells. Our previous observation also demonstrated that activation and nuclear translocation of caspases were associated with prognosis of primary neuroblastomas (Nakagawara *et al.*, 1997). Therefore, the molecular mechanism(s) of RA-induced activation of caspases in neuroblastoma cells needs to be clarified.

In response to a variety of apoptotic stimuli, p53 is induced to be stabilized and subsequently transactivates a number of proapoptotic genes that encode Bcl-2

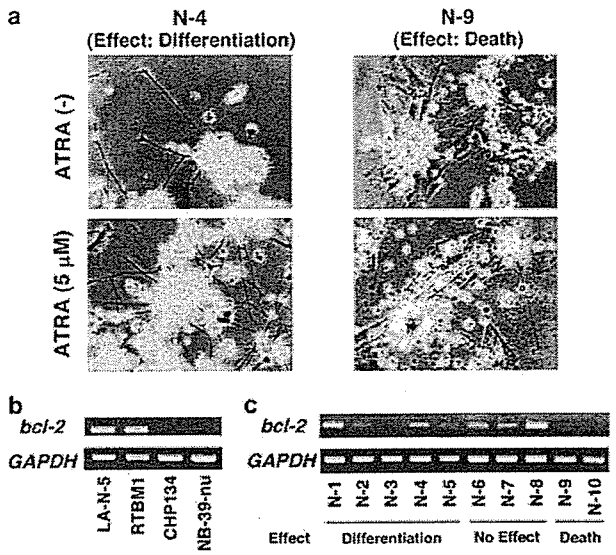

Figure 5 Primary culture and *bcl-2* expression of sporadic neuroblastomas. (**a**) Primary tumor cells prepared from 10 sporadically found neuroblastoma tissues were cultured with or without 5 μM of ATRA. After 4 days, cells were examined by phase-contrast microscope, and morphological changes of two representative cases are shown. (**b** and **c**) RT–PCR analysis. Total RNA was purified from the indicated neuroblastoma cell lines (**b**) and fresh-frozen tissues of primary neuroblastomas (**c**), and subjected to RT–PCR using specific primers for *bcl-2*. N-1 to N-10 indicates the case numbers, and the effects of ATRA on primary cultures are described at the bottom of this panel. Glyceraldehyde-3-phosphate dehydrogenase (*GAPDH*) expression is shown as an internal control.

family proteins including Bax (Culmsee and Mattson, 2005). It has been well documented that Bax acts on the mitochondria to induce mitochondrial permeability transition, and thereby regulating the cytoplasmic release of cytochrome *c* (Antonsson, 2001). Neuroblastoma cell lines that we examined in this study carry wild-type p53. Under our experimental conditions, however, we could not detect the ATRA-mediated upregulation of the endogenous p53 as well as Bax. Similarly, the p53-responsible $p21^{WAF1}$ and proapoptotic Puma were not accumulated in response to ATRA. As described (Nikolaev *et al*., 2003), p53 might not be functional in neuroblastoma cells due to its abnormal cytoplasmic retention. Consistent with this notion, p53 was predominantly expressed in the cytoplasm of neuroblastoma cells examined in this study (data not shown). We have previously shown that cytoplasmic p53 is translocated into the nucleus of CHP134 cells in response to ATRA (Takada *et al*., 2001); however, our present results suggest that translocated p53 was not functional. Indeed, it is reported that p53 in neuroblastoma cells is not functional even after its enforced translocation into the nucleus (Ostermeyer *et al*., 1996). Thus, it is likely that the ATRA-mediated apoptotic cell death in neuroblastoma cells is regulated in a p53-independent manner.

Among other regulators of mitochondrial pathway of apoptosis, Bcl-2 family proteins are critical determinants of mitochondrial membrane potential, which controls the cytoplasmic release of cytochrome *c* from mitochondria and thereby regulating apoptotic cell death (Cory *et al*., 2003). They are divided into two subfamilies based on their biological roles. Antiapoptotic subfamily includes Bcl-2 and Bcl-x_L and proapoptotic subfamily includes Bax, Bim and Bmf. The balance between these two groups determines the fate of cells. Antiapoptotic Bcl-2 is one of the most important members that inhibits the mitochondria-dependent apoptotic pathway triggered by diverse cytotoxic agents through blocking mitochondrial permeability transition. Indeed, the upregulation of Bcl-2 was associated with the drug-resistant phenotype of certain human tumors (Dole *et al*., 1994; Lombet *et al*., 2001). Most intriguingly, our expression studies revealed that antiapoptotic Bcl-2 was constitutively overexpressed in LA-N-5 and RTBM1 cells, whereas its expression levels were extremely low in CHP134 and NB-39-nu cells. In response to ATRA, Bcl-2 was slightly induced to be accumulated in NB-39-nu cells; however, it was maintained at extremely low levels in CHP134 cells. Furthermore, two primary neuroblastomas on which ATRA had toxic effect in primary culture did not express *bcl-2*, similar to CHP134 and NB-39-nu cells. Interestingly, ATRA induced differentiation in five cases and had undetectable effects on three cases, but cell death was induced in two cases. Considering that RA treatment contributed to survival of 17% of patients with aggressive neuroblastomas (Matthay *et al*., 1999), our present results using primary neuroblastomas seem to be reliable. Taken together, it is likely that ATRA potentially have toxic effect on certain neuroblastoma cells (both primary cells and cell lines) that express little Bcl-2. Our current results also revealed that enforced expression of Bcl-2 in CHP134 cells inhibited the ATRA-mediated apoptosis in association with the activation of caspase-3. Furthermore, ATRA treatment of RTBM1 cells followed by HA14-1 exposure underwent apoptotic cell death through mitochondrial pathway. These observations also support the importance of Bcl-2 in the regulation of apoptotic response of neuroblastoma cells to RA.

Although it is still unclear whether the expression levels of Bcl-2 could be correlated with the prognosis of neuroblastoma patients (Romani and Lu, 1994; Gallo *et al*., 2003; Abel *et al*., 2005), it is possible that Bcl-2 plays a key role at least in part in the regulation of ATRA-mediated apoptotic cell death in neuroblastoma cells. In this connection, the antisense RNA-mediated knockdown of the endogeneous Bcl-2 has been employed to treat certain tumors (Kim *et al*., 2004). Recently, a novel Bcl-2 inhibitor that has an antitumor effect on solid tumors has been developed (Oltersdorf *et al*., 2005). Based on our present findings, the combination of RA with Bcl-2-specific inhibitor might provide a novel therapeutic strategy for the treatment of neuroblastomas, instead of the classical chemotherapy that frequently has multi-organ side effects.

Materials and methods

Cell lines and transfection

Human neuroblastoma-derived cell lines, including LA-N-5, RTBM1, CHP134 and NB-39-nu, were maintained in RPMI 1640 medium supplemented with 10% heat-inactivated fetal bovine serum, penicillin (50 U/ml) and streptomycin (50 μg/ml) at 37°C in a humidified atmosphere of 5% CO_2 in the air. For transfection, CHP134 cells were transfected with the expression plasmid encoding human Bcl-2 or with the empty plasmid by electroporation using a Nucleofector (Amaxa Biosystems, Koeln, Germany) according to the manufacturer's protocol.

Reagents

All-*trans* retinoic acid was purchased from Sigma (St Louis, MO, USA) dissolved in dimethylsulfoxisde (DMSO) at a final concentration of 5 mM, and kept at −80°C. Bcl-2 inhibitor HA14-1 was purchased from Sigma, dissolved in DMSO as a 10 mM stock solution and stored at −20°C. All reagents were of the highest quality available.

Proliferation assay

LA-N-5 and RTBM1 cells were plated in triplicate at a density of 1×10^5 per well in 12-well culture plates. CHP134 and NB-39-nu cells were seeded in triplicate at a density of 1×10^4 in 12-well plates. Twelve hours after seeding the cells, cells were treated with ATRA at a final concentration of 5 μM or left untreated, and medium was replaced every 2 days. At the indicated time points after the treatment with ATRA, cells were trypsinized and number of viable cells was directly scored by using the hemocytometer.

Flow cytometric analysis

Cells were exposed to the indicated concentration of ATRA. At the indicated time points after the treatment with ATRA, cells were collected by brief centrifugation, and fixed with 70% ethanol at −20°C. The cells were washed with phosphate-buffered saline (PBS), resuspended in phosphate-citrate buffer (4 mM citric acid, 200 mM Na_2HPO_4) and kept at room temperature for 15 min. The cells were then centrifuged and resuspended in a solution containing 40 μg/ml of propidium iodide and 0.05% RNase A, and incubated in the dark for 30 min. Before performing flow cytometric analysis, cells were filtered through a 40-μm nylon mesh. DNA content was analysed by FACScan flow cytometer (Becton Dickinson, Oxford, UK).

Immunoblot analysis

Cells were washed twice with ice-cold PBS, lysed in a sodium dodecyl sulfate (SDS)-sample buffer containing 10% glycerol, 5% β-mercaptoethanol, 2.3% SDS and 62.5 mM Tris-HCl, pH 6.8, and then boiled for 3 min. The protein concentrations were determined using Bio-Rad protein assay dye reagent (Bio-Rad Laboratories, Hercules, CA, USA). Bovine serum albumin (BSA) was used as a standard. Aliquots (20 μg) of whole-cell lysates were separated by SDS–polyacrylamide gel electrophoresis and electrophoretically transferred onto polyvinylidene difluoride membranes (Immobilon-P, Millipore, Bedford, MA, USA). The membranes were blocked with 0.3% non-fat milk in Tris-buffered saline containing 0.1% Tween-20 and incubated with appropriate primary antibodies at room temperature for 1 h followed by incubation with the horseradish peroxidase-conjugated secondary antibodies (Cell Signaling Technology Inc., Beverly, MA, USA). Immunoreactive bands were visualized by using ECL system (Amersham Biosciences, Uppsala, Sweden). The primary antibodies used in this study were as follows: polyclonal anti-caspase-12 (Cell Signalling Technology Inc.), polyclonal anti-caspase-3 (Calbiochem, San Diego, CA, USA), polyclonal anti-PARP (Cell Signaling Technology Inc.), polyclonal anti-PUMA (ab9643; Abcam, Cambridge, UK), polyclonal anti-$p21^{WAF1}$ (H-164; Santa Cruz Biotechnology), polyclonal anti-Bim (Cell Signaling Technology Inc.), polyclonal anti-Bmf (Cell Signaling Technology Inc.), polyclonal anti-actin (20-33; Sigma), monoclonal anti-caspase-8 (5F7; Medical & Biological Laboratories, Nagoya, Japan), monoclonal anti-caspase-9 (5B4; Medical & Biological Laboratories), monoclonal anti-p53 (DO-1; Oncogene Research Products, Cambridge, MA, USA), monoclonal anti-Bax (6A7; eBioscience, San Diego, CA, USA), monoclonal anti-Bcl-2 (100; Santa Cruz Biotechnology); and monoclonal anti-Bcl-x_L (H-5; Santa Cruz Biotechnology) antibodies.

Immunofluorescent staining

CHP134 cells were grown on coverslips in standard culture medium in the presence or absence of 5 μM of ATRA for 4 days. Cells were washed with ice-cold PBS, fixed with 3.7% formaldehyde in PBS for 30 min, permeabilized with 0.2% Triton X-100 in PBS for 5 min and then blocked with 3% BSA in PBS for 1 h at room temperature. After blocking, cells were incubated with a monoclonal antibody against cytochrome *c* (6H2.B4; BD PharMingen, San Jose, CA, USA) or with a normal mouse IgG for 1 h at room temperature, followed by the incubation with fluorescein isothiocyanate-conjugated secondary antibody against mouse IgG (Santa Cruz Biotechnology). The cell nuclei were stained with DAPI. The coverslips were mounted onto glass slides, and the stained cells were examined by using a confocal laser scanning microscope (Olympus).

Primary culture

RPMI 1640 medium supplemented with 10% heat-inactivated fetal bovine serum, penicillin (50 U/ml), streptomycin (50 μg/ml) and 100 μg/ml of OPI (Sigma) was used as a standard medium for primary culture. Primary tumor cells were prepared from fresh human neuroblastoma tissues by a standard method. A total of 5×10^5 cells of each sample were resuspended in 1 ml of the standard medium, and seeded on 24-well tissue culture plates precoated with collagen. The cells were treated with or without ATRA at a final concentration of 5 μM for at least 2 weeks. The effects of ATRA on the growth and neurite extension of primary neuroblastoma cells were examined by phase-contrast microscope.

RNA extraction and RT–PCR

Total RNA was prepared from fresh-frozen tissues of primary neuroblastomas or cultured cells by using RNeasy Mini Kit (Qiagen, Valencia, CA, USA). Total RNA (2 μg) was reverse transcribed by using random primers and SuperScript II reverse transcriptase (Invitrogen, Carlsbad, CA, USA). The resultant cDNA was subjected to PCR-based amplification. The oligonucleotide primers used in this study were as follows: *bcl-2*, 5′-GAGGATTGTGGCCTTCTTTG-3′ (forward) and 5′-ACAGTTCCACAAAGGCATCC-3′ (reverse), and glyceraldehyde-3-phosphate dehydrogenase (*GAPDH*), 5′-ACCTGACCTGCCGTCTAGAA-3′ (forward) and 5′-TCCACCACCCTGTTGCTGTA-3′ (reverse). PCR products were electrophoretically separated on 1% neutral agarose gels and visualized by ethidium bromide staining.